



School of Chemistry

**Investigation into the Effect of Heating CVD  
Diamond on the Efficacy of Oxygen and  
Hydrogen Termination Achieved Using a DC  
Plasma Reactor**

By George Smith

**This thesis was submitted on the 15<sup>th</sup> of April 2019 in partial fulfilment of the requirements for the Honours Degree of BSc Chemistry at the University of Bristol.**

Supervisor: Professor Paul May  
Second Assessor: Dr. Neil Fox  
Physical and Theoretical

## Acknowledgments

---

I would like to thank Ed Smith, Michael James and Fabian Fogarty for their constant guidance and time taken to teach me how to use all the equipment, along with making me feel welcome in the Diamond Lab. Thanks also to Dr. James Smith and Ed Aldred for assisting in installation of the heating system, and patiently helping when the reactor frequently malfunctioned. I would also like to extend my gratitude to Professor Paul May for offering support and guidance throughout the project.

Thank you also to Klara and my mum for keeping me motivated and providing me much needed emotional support.

## Abstract

---

Research into the termination of diamond films has opened up countless possibilities for applications, spanning multiple fields. Due to hydrogen rich reaction conditions, CVD diamond results in hydrogen surface termination. This has been widely studied due to the interesting property of negative electron affinity (NEA). Using a variety of wet and dry methods, the labile hydrogen atoms can be exchanged with elements such as oxygen, nitrogen or halogens. The new surface atoms can affect structure and electronic properties. However, for a variety of reasons, it is also important to be able to revert to the hydrogen-terminated surface.

Diamond films were grown using the hot filament (HF) (CVD) method, prior to surface manipulation. Laser Raman spectroscopy and scanning electron microscopy were used to characterise the diamond films. These confirmed a uniform polycrystalline diamond film with small defects, originating from manual abrasion as a nucleation method.

Subsequently, custom-built DC Plasma Termination (DCPT) reactor was modified to allow heating of the substrate during termination. This was used to investigate the effect of substrate temperature on efficacy of producing an oxygen or hydrogen termination. The sessile drop method for measuring water contact angles was used to assess the effective termination of the diamond films.

Heating of the diamond substrate was found to inhibit oxidation of the diamond surface. Exposing the diamond film to an oxygen plasma for 7 s at room temperature was the most effective conditions for oxygen termination. Increasing substrate temperature vastly increased efficacy of hydrogen termination. Control samples, hydrogen terminated using a microwave (MW) CVD reactor, were used for comparison. None of the terminations executed in the DCPT reactor reached the hydrophobicity of these control samples. However, some conditions resulted in contact angles that mirrored literature values for hydrogen-terminated polycrystalline diamond films. This suggests a full or almost full hydrogen surface coverage, although further tests such as x-ray photoelectron spectroscopy (XPS) would be required to determine values for surface coverage. Contact angle measurements were quite varied, even among the same sample. This is likely due to use of polycrystalline diamond film, and could have been avoided by using single crystal diamond. Repeat experiments were completed for

conditions that resulted in the most hydrophobic surface. These were; 180 s plasma time, 120 °C; 600 s plasma time, 120 °C; and 600 s plasma time, 200 °C. However, the subsequent contact angles were considerably lower than for the original samples.

## Table of Contents

---

Acknowledgments .....	2
Abstract.....	3
<b>1. – Introduction - Surface Termination of Diamond.....</b>	<b>7</b>
<b>1.1 - Properties of Diamond .....</b>	<b>7</b>
<b>1.2 - Synthetic Diamond .....</b>	<b>8</b>
<b>1.2.1 – Chemical Vapour Deposition Diamond .....</b>	<b>8</b>
<b>1.3 - Diamond Surface Structure .....</b>	<b>9</b>
<b>1.3.1 - (100) Surface.....</b>	<b>10</b>
<b>1.3.2 - (111) Surface.....</b>	<b>11</b>
<b>1.4 - Diamond Termination .....</b>	<b>12</b>
<b>1.4.1 - Hydrogen Termination.....</b>	<b>12</b>
<b>1.4.2 - Oxygen Termination.....</b>	<b>14</b>
<b>1.4.3 - Fluorine Termination .....</b>	<b>17</b>
<b>1.4.4 - Chlorine Termination.....</b>	<b>18</b>
<b>1.4.5 - Nitrogen Termination.....</b>	<b>19</b>
<b>1.4.5.1 - Functionalisation of Nitrogen Terminated Diamond.....</b>	<b>20</b>
<b>1.4.5.2 - Suzuki Coupling .....</b>	<b>21</b>
<b>1.4.6 - Oxygenated Diamond Bound to Metal .....</b>	<b>22</b>
<b>1.5 – Analysis of Terminated Diamond Surfaces.....</b>	<b>24</b>
<b>1.5.1 – Wettability .....</b>	<b>24</b>
<b>1.5.2 - Surface Roughness.....</b>	<b>25</b>
<b>2. – Material Preparation and Experimental Techniques.....</b>	<b>27</b>
<b>2.1 – Project Aim .....</b>	<b>27</b>
<b>2.2 – Preparation of CVD diamond Samples .....</b>	<b>27</b>
<b>2.2.1 – Preparation of Substrate .....</b>	<b>27</b>
<b>2.2.2 – Hot Filament CVD Reactor.....</b>	<b>27</b>
<b>2.2.2.1 – Standard Operating Procedure.....</b>	<b>30</b>
<b>2.2.3 – Hydrogen Termination Using the Microwave Plasma Reactor .....</b>	<b>30</b>
<b>2.3 – DC Plasma Termination Reactor.....</b>	<b>31</b>
<b>2.3.1 – Modifications .....</b>	<b>33</b>
<b>2.3.2 – Heater Calibration .....</b>	<b>34</b>
<b>2.3.3 – Standard Operating Procedure .....</b>	<b>35</b>
<b>2.4 – Analysis of the Terminated Surface.....</b>	<b>36</b>

2.4.1 – Contact Angle Measurements .....	36
3. – Results and Discussion.....	38
3.1 – Scanning Electron Microscopy .....	38
3.2 – Laser Raman Spectroscopy .....	39
3.3 – Contact Angle Measurements .....	41
3.3.1 – Oxygen Termination .....	41
3.3.2 – Hydrogen Termination .....	43
3.3.2.1 – Reproducibility .....	46
3.3.2.2 – Discrepancies.....	46
4. – Conclusion .....	49
5. – Further Work .....	51
5.1 – X-Ray Photoelectron Spectroscopy.....	51
5.2 - Surface Position .....	51
5.3 - Cooling .....	52
5.4 - Nitrogen Termination .....	52
6. – References .....	54

# 1. – Introduction - Surface Termination of Diamond

---

## 1.1 - Properties of Diamond

Since their discovery, dating back millennia, diamonds have been close to the hearts of the general public and the scientific community alike. For the average consumer, diamond is mainly used for adornment and is seen as a symbol of wealth, commitment and love. However, in the scientific community, it is the vast and impressive properties of diamond that make this carbon allotrope so fascinating.

Diamond is a metastable allotrope of carbon, in which the carbon atoms are  $sp^3$  hybridised in a tetrahedral network. Each carbon atom is at the centre of four other carbon atoms forming a face-centred cubic arrangement with half-filled tetrahedral vacancies<sup>[1]</sup>. The cubic lattice structure is what makes diamond exceptionally hard, and imbues it with other useful properties. A few of the most important are listed in Table 1. These properties give diamond a vast array of industrial applications. The unrivalled hardness of diamond makes it perfect for cutting and abrasive tools. It is also heavily utilised in electronics as a heat sink, due to the high thermal conductivity, coupled with low thermal expansion<sup>[2]</sup>. Also, the large optical transparency makes it a perfect choice for optics<sup>[3]</sup>.

**Table 1: Important properties that make diamond suitable for a wide range of industrial applications<sup>[1]</sup>.**

Property	Value	Unit
Hardness	$1.0 \times 10^4$	kg mm <sup>-2</sup>
Strength, tensile	>1.2	GPa
Strength, compressive	>110	GPa
Density	3.52	g m <sup>-3</sup>
Young's modulus	1.22	GPa
Thermal conductivity	$2 \times 10^3$	W m <sup>-1</sup> K <sup>-1</sup>
Thermal expansion coefficient	$1.1 \times 10^{-6}$	K <sup>-1</sup>
Electron affinity	Negative	On H-terminated surface
Optical transparency	From deep UV to far IR	N/A

## 1.2 - Synthetic Diamond

Although it is possible to cleave natural diamonds to fit a desired purpose, the size and shape is still limiting for many applications. The majority of diamonds used in industry are made using the high pressure high temperature (HPHT) method<sup>[4]</sup>. This method relies on subjecting carbon to conditions that make the diamond structure the thermodynamically favoured form (temperature ~1500-2000 °C, pressure ~5-10 GPa)<sup>[5]</sup>.

### 1.2.1 – Chemical Vapour Deposition Diamond

There is a need for a more controlled and versatile method of forming synthetic diamond. Chemical vapour deposition (CVD) is a method that has been widely researched since the 1960s, gaining vast momentum due to work by John C. Angus and Cliff C. Hayman in 1988<sup>[6]</sup>. The driving force for this method is kinetics rather than thermodynamics.

In CVD, heat or plasma is utilised to ionise and break up a gaseous mixture of predominantly hydrogen and a small quantity of methane. A gas phase reaction then occurs above the solid surface, resulting in diamond formation. Hydrogen atoms terminate the dangling carbon bonds, preventing reconstruction to graphitic carbon. As the bond strength of C-H is greater than C-C, hydrogen radicals are required to facilitate removal of these terminating hydrogen atoms in order to allow further growth. This creates a vacant site which a carbon-containing radical can bond to, extending the diamond film, atom-by-atom. Other carbon allotropes, such as graphite, form under CVD growth conditions. However, hydrogen radicals etch these forms of carbon at a faster rate than growth occurs, whilst the converse is true for the diamond allotrope. The benefits of this method is that polycrystalline diamond can be formed in controlled shapes or patterns and across large substrate surfaces. Also, other gases may be added to the reaction chamber to create doped diamond films. The concentration of dopant within the film is easily controlled by altering the concentration of prerequisite gas<sup>[7]</sup>.

### 1.3 - Diamond Surface Structure

Where a diamond is cleaved or has finished forming, there is a surface of dangling bonds exposed. Diamond forms three predominant surface structures which can be depicted by the Miller indices, (100), (110) and (111). These are shown in Fig. 1a<sup>[8]</sup>. Cleavage along these planes result in the crystal structure shown in Fig. 1b. The crystal structures have been reoriented so that the c-axis for each structure is aligned. Synthesising diamond by the HPHT and CVD methods rarely leads to the (110) surface structure. This is due to the (110) surface being the fastest growing surface, and hence grows out<sup>[9]</sup>. The (100) and (111) surfaces both undergo reconstruction to form an alternative crystal structure to the bulk layers.

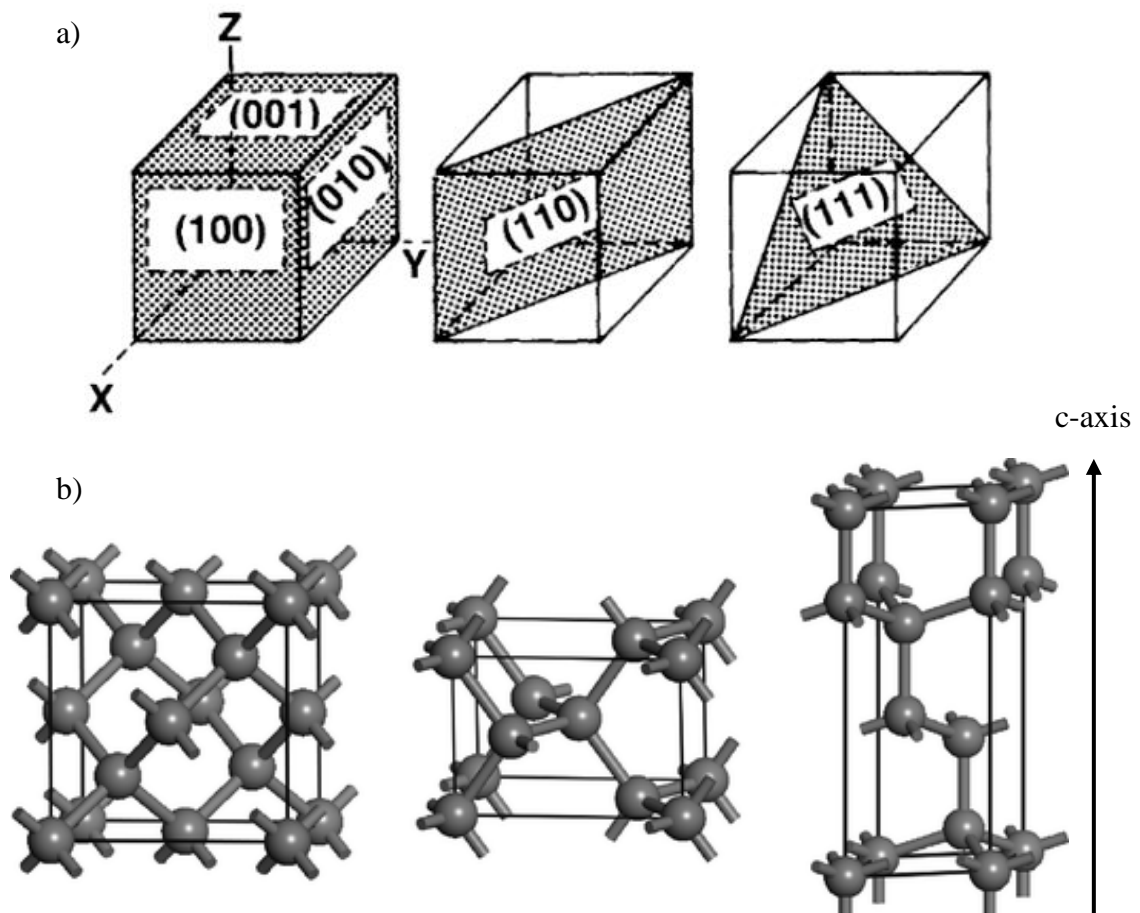


**Figure 1: a) Image depicting the Miller indices corresponding to the main cleavage planes in diamond<sup>[10]</sup>. The resultant crystallographic planes of diamond are shown in b). Left – (100), middle – (110), right – (111)<sup>[11]</sup>.**

### 1.3.1 - (100) Surface

The (100) diamond surface has two dangling bonds per surface atom. On the clean (100) diamond surface, adjacent carbon atoms rearrange to form double-bonded dimers, in order to remove dangling bonds and lower the energy. This results in a  $(2 \times 1)$  reconstruction in which each surface atom has adopted a distorted  $sp^3$ -like coordination<sup>[12]</sup>. Theoretical predictions suggest the formation of the dimers introduces occupied  $\pi$  and unoccupied  $\pi^*$  states reducing the bandgap to 1.3 eV, inducing semiconducting properties in the material<sup>[9],[13]</sup>. However, CVD diamond growth takes place in a hydrogen rich atmosphere creating a  $(1 \times 1)$  surface of dihydride carbon atoms. In this formation, the terminal hydrogen atoms are in closer proximity than in gaseous hydrogen. To remove steric hindrance, and hence lower the energy, the surface undergoes reconstruction similar to that of the clean surface. The new structure adopts parallel rows of symmetric mono-hydrogenated dimers<sup>[14]</sup>. This can be seen clearly in Fig. 2. The  $(2 \times 1)$  symmetry is also confirmed by low energy electron diffraction (LEED)<sup>[15]</sup>.

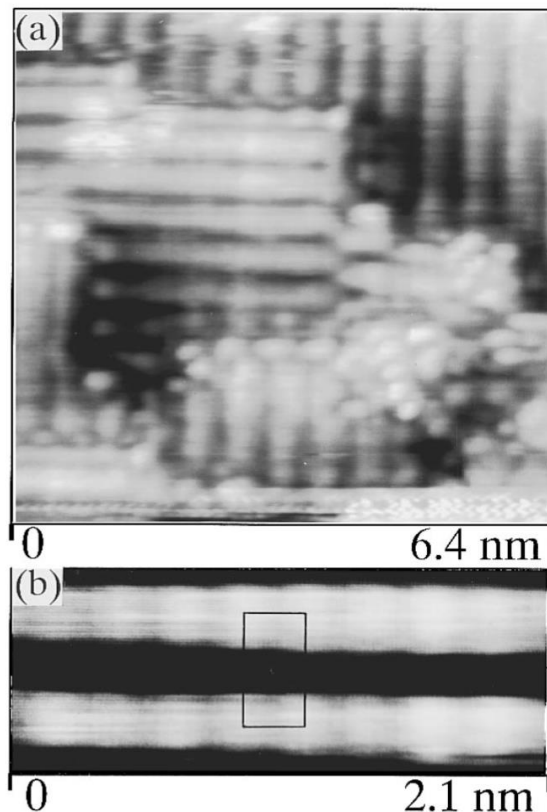


**Figure 2: (a) Scanning tunnelling microscopy (STM) atomic resolution image of a CVD grown epitaxial diamond (100) film, after  $(2 \times 1)$  surface reconstruction. (b) Close-up of image showing individual  $(2 \times 1)$  rows of dimers that occur to stabilise the surface structure<sup>[16]</sup>.**

### 1.3.2 - (111) Surface

The (111) surface is often referred to as cubic, due to the atoms being arranged in the cubic close packing (ccp) arrangement. The crystal adopts an ABCABC structure, meaning every third layer is the same. In order to obtain the (111) surface, one or three bonds are cut per surface atom, creating a  $(1 \times 1)$  single-dangling-bond surface. However, unless under extreme conditions, the one dangling bond is generally the natural cleavage plane. On a clean carbon face, this structure is unstable due to the dangling bonds. The surface reconstructs to form the  $\pi$ -bonded  $(2 \times 1)$  Pandey-chain model similar to the Si(111) reconstruction<sup>[14]</sup>. The carbon atoms form zigzag chains parallel to one another. The surface carbon atoms are only coordinated to three other carbon atoms, creating a delocalised  $\pi$  network through the chains. This means the surface of this particular structure displays semi-metallic properties<sup>[9]</sup>. However, hydrogenation of the terminal C atoms stabilises the (111)  $(1 \times 1)$  formation, up to temperatures of  $\approx 1100$  K<sup>[14]</sup>. As shown in Fig. 3, the (111) surface can be grown almost atomically smooth. This makes it of great interest in the scientific community<sup>[17]</sup>.

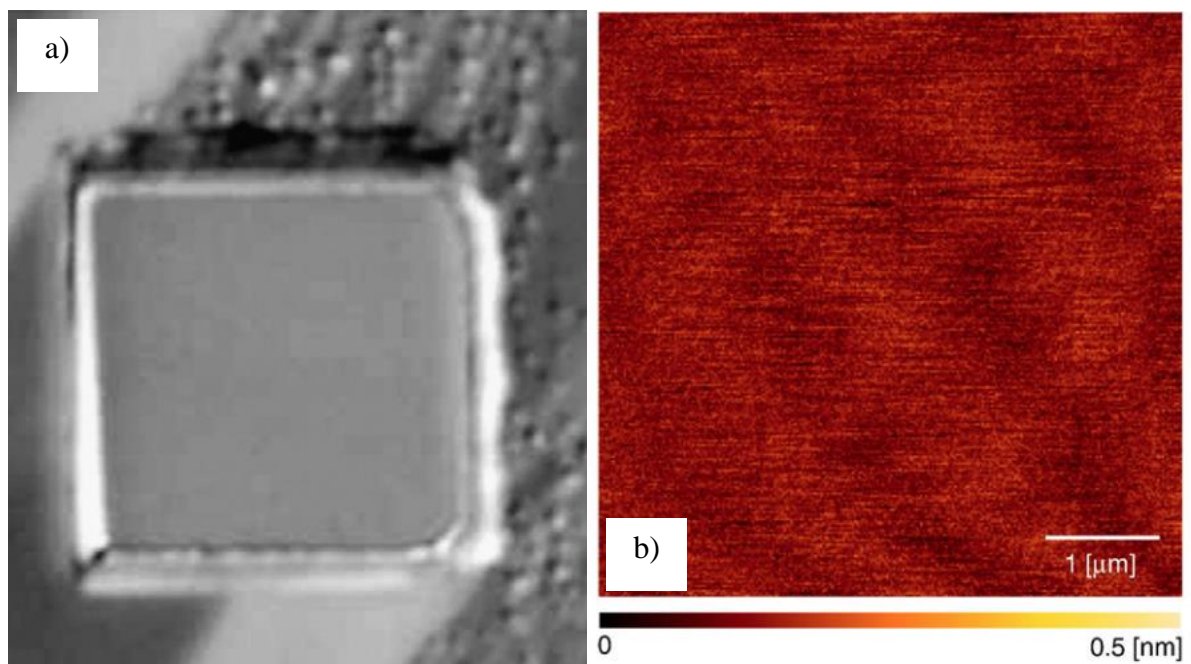


**Figure 3: a) Optical microscopy (OM) image of a (111) CVD diamond film. b) Atomic force microscopy (AFM) image of the same diamond (111) surface. The AFM image gives a root mean square value of 0.03 nm, largely due to limitations with the AFM system, indicating an extremely smooth surface<sup>[18]</sup>.**

## 1.4 - Diamond Termination

As previously mentioned, diamond grown using CVD methods is hydrogen terminated due to the hydrogen-rich reaction chamber atmosphere. Using wet and dry chemical methods, these labile C-H terminal bonds can be broken and the hydrogen atoms exchanged with a wide range of other atoms or groups of atoms. Surfaces and interfaces often govern functional properties of a material, and diamond is no different. Terminating the diamond film with these different atoms can vastly change the properties of the diamond film, including the electron affinity, hydrophobicity, or conductivity<sup>[19]</sup>.

### 1.4.1 - Hydrogen Termination

For the diamond (111) surface, hydrogenation can occur for both the  $(1 \times 1)$  single dangling bond surface (Fig. 4a) and the  $(2 \times 1)$  Pandey-chain reconstruction. However, *ab initio* calculations have shown that of these two, the unreconstructed  $(1 \times 1)$  surface is 0.70 eV lower in energy per surface C-H pair<sup>[9]</sup>.

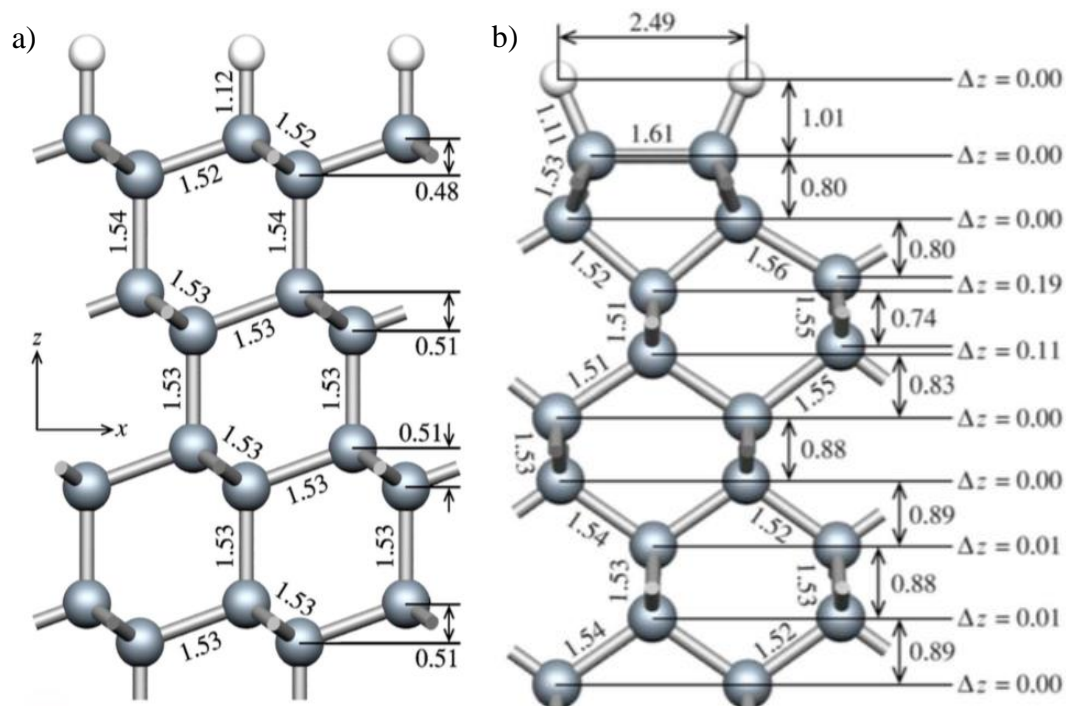


**Figure 4: Stable structures of hydrogen-terminated diamond. a) – the (111) unreconstructed  $(1 \times 1)$  structure. b) – the (100)  $(2 \times 1)$  dimer reconstruction. All measurements are in Å<sup>[9]</sup>.**

For a hydrogen-terminated diamond (100) surface, the most stable form is the  $(2 \times 1)$  monohydrogenated  $\pi$ -bonded reconstruction (Fig. 4b). On the clean (100) surface, the terminal carbon atoms form doubled-bonded dimers. Addition of hydrogen to these carbon atoms removes the  $\pi$  and  $\pi^*$  states, and the dimers instead become single bonded<sup>[9]</sup>.

Hydrogen termination on diamond occurs naturally alongside oxygen termination due to both being present in air. Methane and hydrogen gas are typically used as a precursor gas in excess of hydrogen for CVD growth<sup>[8]</sup>. This results in the hydrogen terminated surface being the dominant form for CVD diamond films. It is also possible to prepare hydrogen-terminated diamond from other diamond terminations. Some of these methods are; exposing the film to hydrogen plasma, or annealing to high temperatures, before exposure to hydrogen gas<sup>[20],[21]</sup>. Although the hydrogenated diamond surface is quite stable, surface hydrogen atoms are displaced by oxygen at room temperature<sup>[22]</sup>. However, this process is very slow. It has been reported that heating the surface to 300 °C in air causes oxidation of the surface, and heating to 480 °C results in burning of the diamond surface<sup>[23]</sup>.

Hydrogen-terminated diamond is of particular interest, due to the surface acting as a p-type semiconductor, and possessing the unusual property of negative electron affinity (NEA)<sup>[19]</sup>. NEA can occur when the vacuum energy level lies below the conduction band minimum, allowing electrons to dissipate easily from the surface of the material<sup>[24]</sup>. There are two possible forms of NEA that can be displayed by a material. These are known as true or effective NEA (Fig. 5). Effective NEA occurs as a result of positive electron affinity and strong downward band-bending at the surface, causing the conduction band minimum to be below the vacuum level<sup>[25]</sup>. Effective NEA can be quantified using Eq. 1, where  $\varphi_{BB}$  is the magnitude of band bending and  $\chi$  is electron affinity. True NEA is caused by a dipole layer at the surface of the semiconductor surface. In this situation, the depletion band increases the NEA effect; therefore Eq. 2 must be used to calculate a true NEA<sup>[26]</sup>. Fig. 5 shows a visual representation of the band levels required for true and effective negative electron affinity.

$$\chi_{eff} = \varphi_{BB} - \chi \quad (\text{Eq. 1})$$

$$\chi_{true} = \varphi_{BB} + \chi \quad (\text{Eq. 2})$$

Hydrogen-terminated diamond has a true NEA surface. As mentioned above, this can be explained by examining the surface dipole arising from the difference in electronegativity between the hydrogen and carbon atoms. Hydrogen and carbon have electronegativity values of 2.20 and 2.55, respectively<sup>[27]</sup>. While difference between these values is not large, this still causes a  $C^{\delta-}-H^{\delta+}$  surface dipole, where  $\delta$  is the partial charge on the atom. This dipole bends the conduction band down further with respect to the vacuum, causing an experimental NEA value of -1.30 eV<sup>[28],[29]</sup>.

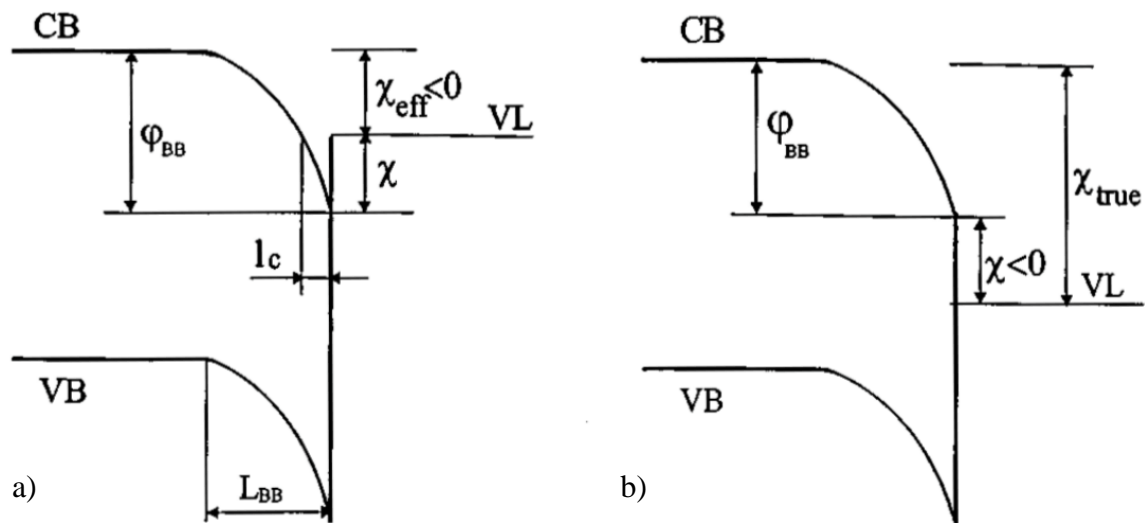


**Figure 5: General band diagram of the surface of a semiconductor for effective NEA (a) and true NEA (b). CB, VB and VL are conduction band, valence band and vacuum level, respectively.  $L_{BB}$ ,  $\phi_{BB}$ ,  $\chi$ ,  $\chi_{true}$  and  $\chi_{eff}$  are defined as the depletion layer, magnitude of band bending, electron affinity, true electron affinity and effective electron affinity<sup>[26]</sup>.**

#### 1.4.2 - Oxygen Termination

On the diamond (111) surface, there are two predominant ways to incorporate oxygen into the surface structure; bridged oxygen (ether) and ketone. If hydrogen is present, a hydroxyl and carboxyl group are also possible<sup>[30]</sup>. *Ab initio* calculations have shown the most stable form to be the  $(1 \times 1)$  ketone formation with each carbon atom  $\pi$ -bonded to an oxygen atom<sup>[31]</sup>. Oxygen can also be absorbed on to the  $(2 \times 1)$  clean surface at low oxidation temperatures and still retain structure. Calculations reveal an optimised  $(2 \times 1)$  surface where an oxygen is bonded to two carbon atoms on the Pandey-chain, with the neighbouring carbon dimer in the chain not bonded to oxygen. This only gives a 50 % oxygen coverage. Accommodating a full monolayer

of oxygen breaks the Pandey-chain in order to  $\pi$ -bond to the oxygen atoms. To achieve this, the surface reconstructs into the lower energy,  $(1 \times 1)$  structure<sup>[31]</sup>.

For the diamond  $(100)$  surface, oxygen can be incorporated in similar ways to the  $(111)$  surface; ether, ketone, and in the presence of hydrogen, hydroxyl and carboxyl functional groups. These are shown below, in Fig. 5. Both the ether and ketone formation mean the carbon atoms are no longer dimerised as in the clean  $(100)$  surface. *Ab initio* calculations conclude that the ether formation is 0.60 eV per oxygen atom lower in energy than the carbonyl<sup>[9]</sup>. However, in practice for an oxygen rich atmosphere, a combination of the ketone and ether functional groups are formed. For lower oxygen coverage, high-resolution electron loss spectroscopy (HREELS) studies predict the ketone form dominates. However, for high surface coverage, the ether formation is the primary terminating species<sup>[32]</sup>.

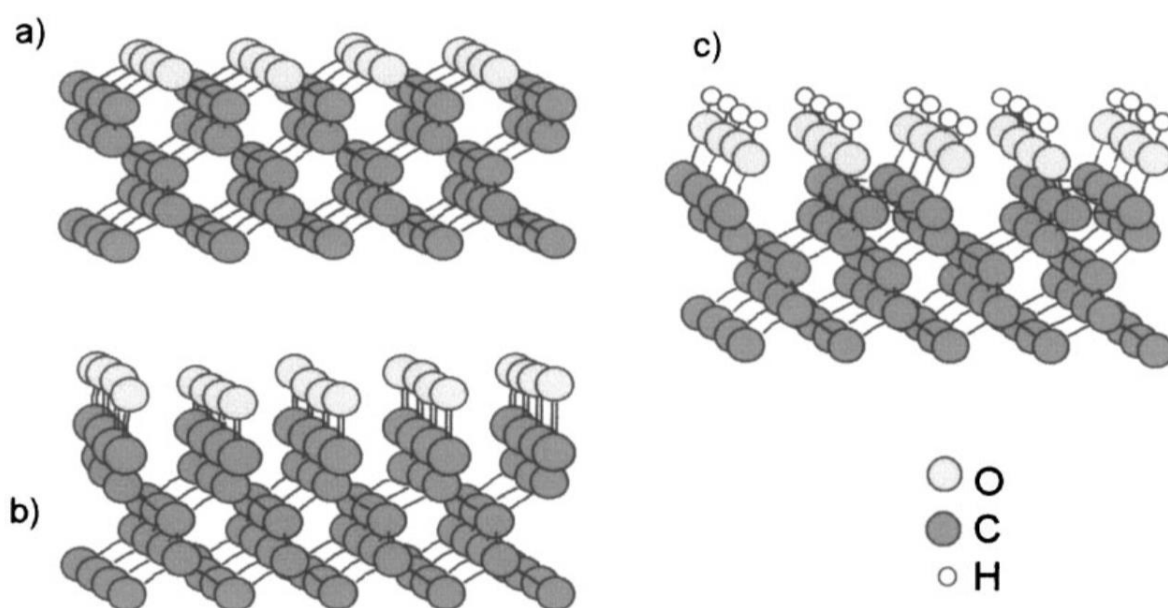


**Figure 6: The three possible structures for oxygen incorporated into the  $(100)$  surface. a) bridged oxygen (ether) b)  $\pi$ -bonded oxygen (ketone) c) hydroxyl (C-OH)<sup>[33]</sup>.**

*Ab initio* calculations have shown the most stable form of hydroxyl group coverage on the  $(100)$  surface is the  $(2 \times 1)$  reconstruction where an OH group is attached to each carbon atom in the dimer from the clean surface. It has been shown that there are two possible configurations for the directions of the OH groups, *para* and *anti*, both of which are shown in Fig. 7. The *para* configuration corresponds to the OH groups all pointing in the same direction, parallel. In the *anti* configuration the OH groups are pointing in the opposite direction, antiparallel. The *anti* configuration is calculated to be 21.3 meV lower in energy per surface OH group. This is a

result of the H atoms being further apart in the anti configuration. The surface is stabilised in both of these configurations by significant hydrogen bonding between the highly polarised  $O^{\delta-}-H^{\delta+}$  groups<sup>[9]</sup>.

Heating the oxygen-terminated surface to 300 °C in air strongly decreased the oxygen coverage. Oxygen is desorbed from the surface as oxygen-carbon compounds, mainly CO and CO<sub>2</sub>. This desorption continued to occur up to 600 °C due to the different bond energies for different oxygen functional groups<sup>[34]</sup>. This process etches the diamond surface due to the desorption of the attached carbon atoms<sup>[31]</sup>.

Oxygen-terminated diamond can be produced by several techniques. The main methods utilised include thermal, electrochemical, wet chemical and plasma oxidation<sup>[35]</sup>.

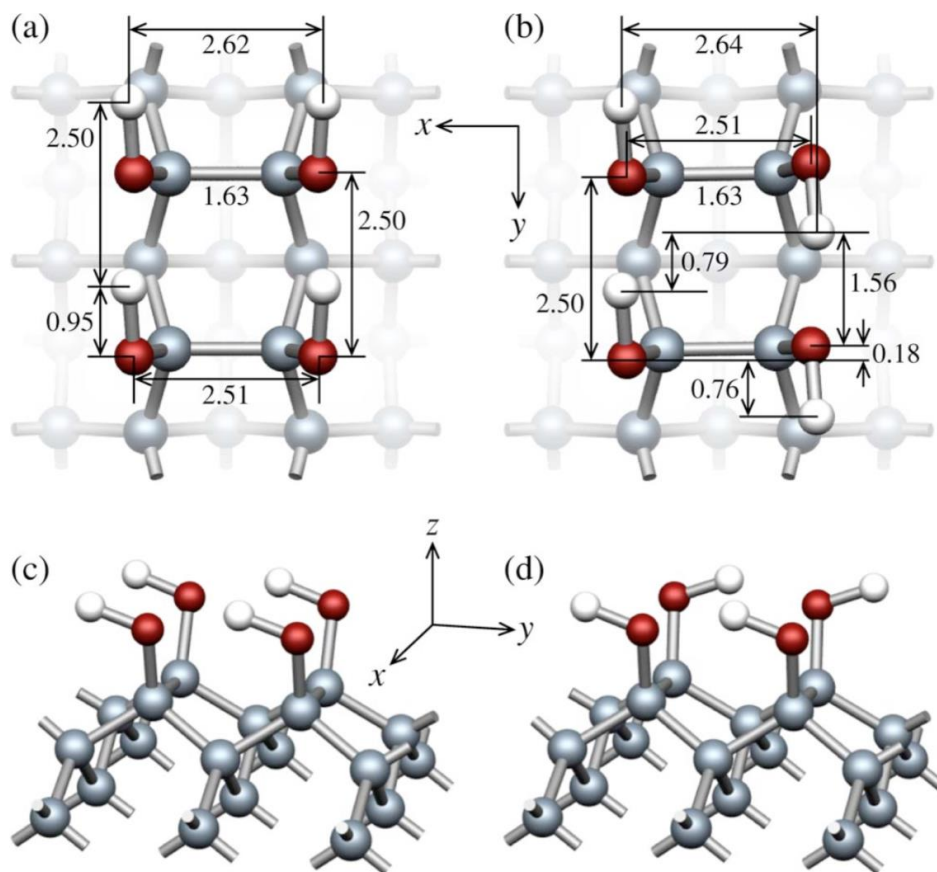


**Figure 7: Geometries for the stable (100) (2 x 1) OH diamond surface. (a) and (c) show the para configuration in plan and perspective view. (b) and (d) show the anti configuration<sup>[9]</sup>. All measurements given in Å.**

Terminating diamond with oxygen changes the film from having a NEA, as with hydrogen-terminated diamond, to a positive electron affinity (PEA). Similar to hydrogen-terminated diamond, this can be explained by looking at the polarity of the surface bonds. Carbon and oxygen have electronegativity values of 2.55 and 3.44<sup>[27]</sup>. Oxygen is very electronegative causing a  $C^{\delta+}-O^{\delta-}$  surface dipole. This polarity results in upwards band bending, and thus, a PEA measured experimentally as 1.70 eV<sup>[28]</sup>.

### 1.4.3 - Fluorine Termination

Due to the large electronegativity difference between fluorine and carbon (3.98 and 2.55, respectively)<sup>[27]</sup>, and fluorine's small van der Waals radius atomic radius (1.4 Å), it is able to form strong covalent bonds to carbon. Furthermore, the van der Waals radius is only slightly larger than that of hydrogen (1.2 Å), allowing easy substitution of hydrogen to form a partial or full fluorine coverage on the diamond surface<sup>[36]</sup>. Similar to that of hydrogen-terminated diamond, the (100) surface undergoes a  $(2 \times 1)$  reconstruction to form a surface of mono-fluorinated carbon atoms (Fig. 8)<sup>[37]</sup>. In a surface of 100 % fluorine coverage, the C-F equilibrium bond length is calculated to be 1.36 Å. This is marginally shorter than the typical C-F bond length of 1.39 Å<sup>[28]</sup>.

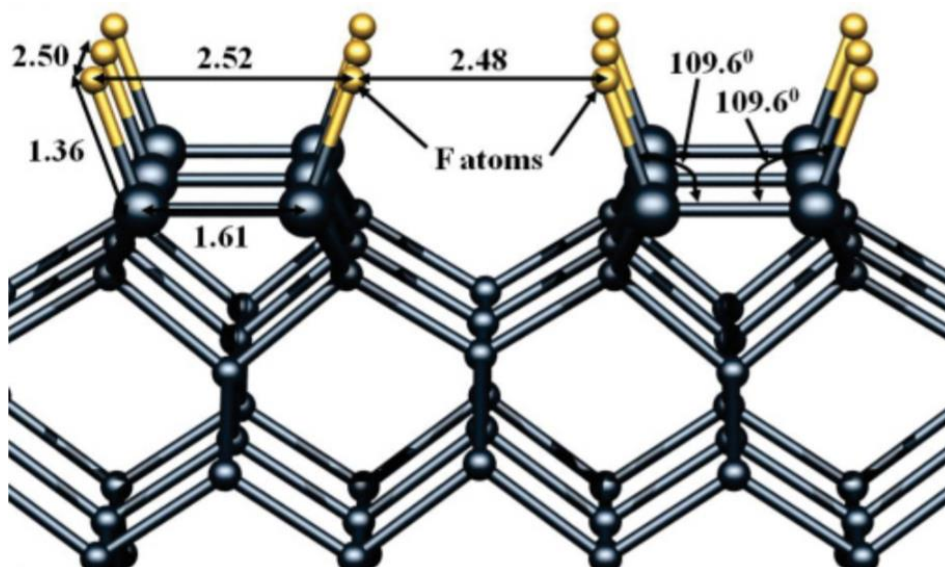


**Figure 8: Calculated structure of 100 percent fluorine coverage on the  $(2 \times 1)$  diamond (100) surface<sup>[28]</sup>. Distance measurements given in Å.**

On the (111) diamond surface, fluorine atoms form  $\sigma$ -bonds with the dangling orbitals on the  $(1 \times 1)$  unreconstructed surface. *Ab initio* calculations suggest that this is the most stable form of fluorine-terminated (111) diamond, rather than the Pandey-chain  $(2 \times 1)$  reconstruction<sup>[38]</sup>. The absorption energy of fluorine onto the (111) surface closely matches the absorption of hydrogen onto a similar surface, at 430 and 431 kJ mol<sup>-1</sup>, respectively<sup>[39]</sup>.

Successful fluorinations of diamond films have been achieved by exposing the surface to atomic fluorine beams, F<sub>2</sub><sup>[40]</sup>, XeF<sub>2</sub><sup>[41]</sup> and fluorocarbons<sup>[42]</sup>, or using plasma containing SF<sub>6</sub> or CF<sub>4</sub> gas<sup>[38]</sup>.

Despite the large dipole moment of the C-F bond, fluorine terminated-diamond is superhydrophobic. In the gas-phase, fluorinated hydrocarbons have been seen to act as hydrogen-bond acceptors and form hydrogen bonds of half the magnitude that water can form to the same proton donors. However, fluorinated hydrocarbons are not observed to form hydrogen bonds when in polar solvents such as alcohols, amines or water. This is believed to be due to the C-F bond being relatively non-polarizable, meaning that dipole-induced dipole, and dispersion interactions between the solvent and the C-F bond are not as favourable as the solvent-solvent interactions<sup>[43]</sup>. This phenomenon is known as polar hydrophobicity, and is found for molecular fluorocarbons, fluorinated diamond, and fluorinated diamond-like carbon surfaces<sup>[36]</sup>.

#### 1.4.4 - Chlorine Termination

Chlorine-terminated diamond forms structures similar to that of fluorine terminated diamond. For the (100) diamond surface, the reconstructed  $(2 \times 1)$  surface is adopted with each carbon terminated with a singular heteroatom. For a surface of 100 % chlorine coverage, the calculated equilibrium C-Cl bond length is 1.72 Å, slightly shorter than the typical C-Cl single bond length of 1.79 Å<sup>[28]</sup>. The structure of this is shown in Fig. 9. However, due to strain caused by the size of the chlorine atoms, 100 % chlorine coverage of the film is not achievable.

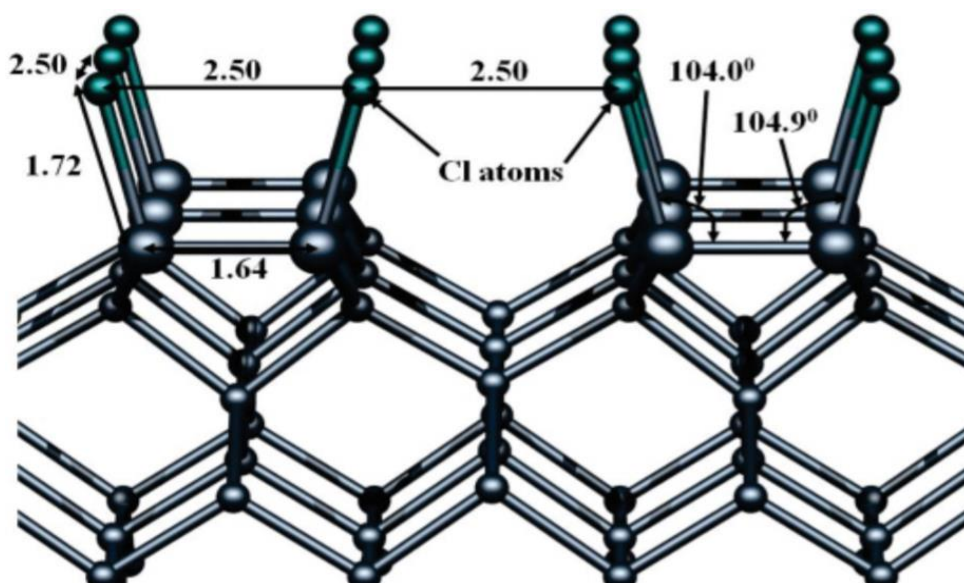


**Figure 9: Calculated structure of 100 % chlorine coverage on the (2 × 1) diamond (100) surface<sup>[28]</sup>. Distance measurements given in Å.**

Similar to fluorine, the (1 × 1) unreconstructed structure for (111) diamond is the most favourable form for chlorine termination. However, the lower electronegativity of chlorine in comparison to fluorine, paired with the larger atomic radius means the absorption of chlorine onto the (111) diamond surface occurs much less readily than for absorption of fluorine or hydrogen onto a similar (111) surface. This can be quantified by looking at the calculated enthalpies of absorption which are 200, 430 and 431 kJ mol<sup>-1</sup>, respectively<sup>[39]</sup>. Due to these differences in energies, the chlorine surface is much less stable than the fluorine and hydrogen surface. Desorption of chlorine from the (111) and (100) surfaces has been recorded to happen from -50 °C to 300 °C, above which chlorine is completely absent from the surface<sup>[30]</sup>.

### 1.4.5 - Nitrogen Termination

There are a variety of different structures that could be formed from amination of a diamond surface. Three main structures have been reported for nitrogen termination; primary amine group (C-NH<sub>2</sub>), imine group (C=NH), and bridged secondary amine group (C<sub>2</sub>-NH). Depending on the acidity of the conditions, protonated analogues of these structures have also been observed (C-NH<sub>3</sub><sup>+</sup>, C=NH<sub>2</sub><sup>+</sup>, C<sub>2</sub>-NH<sub>2</sub><sup>+</sup>). A basic representation for some of the structures mentioned above are shown in Fig. 10. Protonation of the amino groups to form a positively charged surface on the diamond enhances electron emission due to downward bending band bending within the diamond region and electrostatic forces<sup>[44]</sup>.

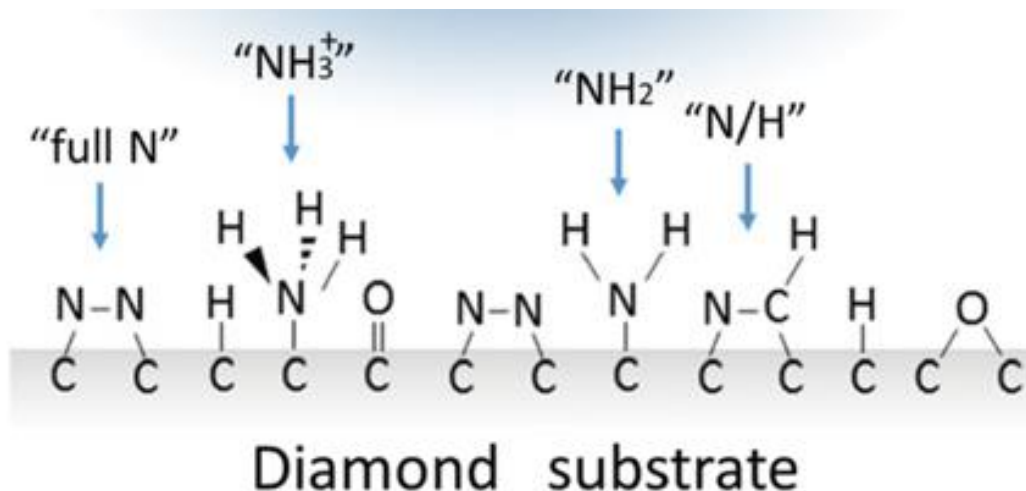


**Figure 10: Basic structural representative of various nitrogen containing and other functional groups on the diamond surface<sup>[45]</sup>.**

It is possible to form these various aminated diamond surfaces by utilising photochemical techniques in the presence of pure ammonia gas. Unlike other surface terminations, little reaction will occur if this process is attempted with hydrogen-terminated diamond. Instead the very reactive, labile chlorine-terminated surface is often required<sup>[46]</sup>. Alternative to this, the diamond surface can be *in-situ* annealed to 1000 °C, forming a bare carbon surface. The surface can then be exposed to a radio frequency N<sub>2</sub> plasma to form terminal nitrogen atoms across the surface<sup>[47]</sup>. Structural analysis of the products for this method have shown alternative structures to those previously mentioned, including a fully nitrogenated surface formed of nitrogen dimers, and an N-C-H structure where nitrogen has replaced a surface carbon atom (shown in Fig. 10). *Ab initio* calculations suggest that the formation enthalpy favours a fully nitrogen-terminated diamond surface<sup>[45]</sup>. Also, for the mixed termination surface (N/C-H), the diamond (111) surface is at least 0.3 eV per atom lower in energy than the diamond (100) surface<sup>[48]</sup>.

#### 1.4.5.1 - Functionalisation of Nitrogen Terminated Diamond

Many biological processes involve the binding of molecules and proteins to receptors. A way to study such interactions is by using biologically sensitive electrical devices<sup>[49]</sup>. Amine groups terminated to the diamond surface possess the same chemical behaviour as ‘free’ amines. Hence, standard organic chemistry can be utilised to couple proteins and DNA to the amine group, immobilising the organic molecules on the diamond solid phase<sup>[50]</sup>. Another way of achieving this is by photochemically grafting terminal alkenes to the hydrogenated diamond surface<sup>[51]</sup>. The modified diamond provides a solid-liquid phase interface, in which the liquid

can be a solution of chosen electrolytes. The semiconducting properties of diamond can be exploited to monitor binding events involving the molecules in the solution and the diamond-bound organic molecules by changes in electrical properties of the diamond phase<sup>[52]</sup>.

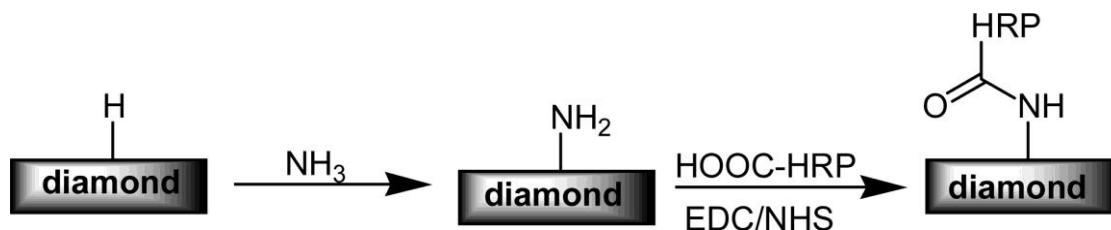


**Figure 11: Schematic diagram illustrating the mechanism for functionalising the diamond surface via amine surface termination. In this case the horseradish peroxidase (HRP) enzyme is attached<sup>[53]</sup>.**

As shown in Fig. 11, enzymes are attached to the nitrogen via an amide bond. In this case the horseradish peroxidase enzyme has been attached<sup>[53]</sup>. However, any organic compound containing a carboxylic acid group could be bonded to the amine surface group.

#### 1.4.5.2 - Suzuki Coupling

Previously mentioned photochemical grafting to the diamond surface is very effective for terminal alkenes not containing other functional groups. However, for biosensors, it is often beneficial to have large organic groups close to the diamond surface, to prevent hydrolysis of the surface bonds on diamond and hence degradation of the sensor. Through  $\pi$ - $\pi$  interactions, aryl groups become much more closely packed than the simple straight alkanes, providing better protection of the diamond surface from the electrolyte solution. However, introducing conjugated aryls as bio-linkers to the diamond surface creates selectivity issues when using photochemical grafting. Suzuki Coupling is a palladium-catalysed reaction employed to synthesis biaryl compounds by cross-coupling aryl halides and aryl boronic acids. A schematic for functionalisation of the diamond utilising the Suzuki reaction is shown in Fig. 12. This reaction provides much higher selectivity and can couple aryl groups to the diamond as a bio-linkers with ease<sup>[54],[55]</sup>.

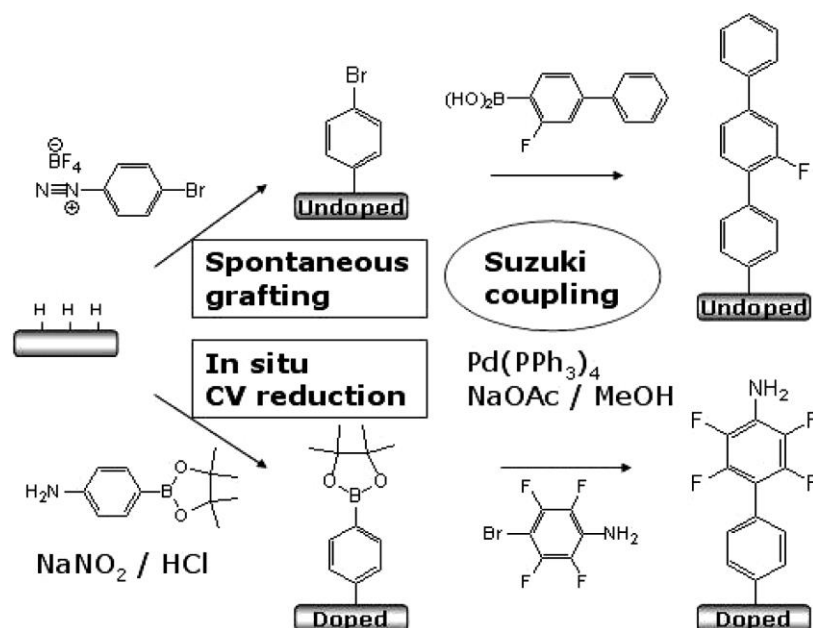


**Figure 12: Two methods for functionalising the diamond surface using aryldiazonium salts, followed by Suzuki Coupling to form biaryl bonds<sup>[54]</sup>.**

#### 1.4.6 - Oxygenated Diamond Bound to Metal

NEA is a property that has been heavily researched in relation to diamond films. NEA in combination with other desirable properties, such as high thermal conductivity and low thermal expansion, makes diamond a promising material for use in photocathodes<sup>[56]</sup>, field emitters<sup>[57]</sup>, and thermionic emitters<sup>[58]</sup>. As previously discussed, the most common form of terminated diamond that displays an NEA is the hydrogen-terminated diamond. This is stable to around temperatures of 740-900 °C, above which hydrogen is desorbed, which is an acceptable temperature limit for thermionic emitters, which require stability at high temperatures<sup>[59]</sup>. However, the surface dipole of the hydrogenated diamond is quite small, leading to a work function in the range of 2.85 to 3.9 eV. For lower temperature thermionics, a work function close to 1 eV is optimal<sup>[25],[59]</sup>. Hydrogen-terminated diamond is also susceptible to chemical and electronic degradation, both resulting in reduced electron emission yield<sup>[49]</sup>. Hence, discovery of new diamond materials which are both highly polar and thermally stable are of interest.

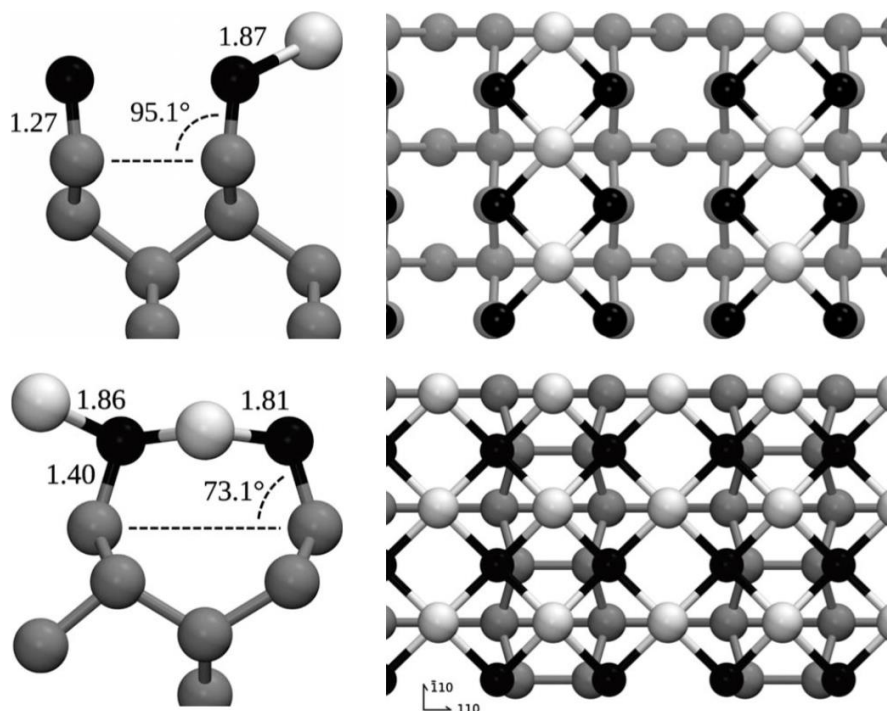


**Figure 13: *Ab initio* calculated lowest energy structures in section and plan views for 0.5 ML (top) and 1.0 ML (bottom) lithium adsorption on C(100) (1 × 1):O<sup>[59]</sup>.**

One method found of inducing a NEA is depositing a monolayer (ML) of light metals onto the clean or the oxygen-terminated diamond surface. These materials are shown to be much more stable to chemical and electronic degradation. Lithium deposited onto the clean and oxygenated diamond surface is the most researched. *Ab initio* calculations predict for adsorption of lithium onto the clean (100) (2 × 1) surface, an NEA of -1.45 eV and -2.7 eV, corresponding to a 0.5 and 1 lithium ML, respectively<sup>[59]</sup>. Lithium adsorbed onto the oxygenated diamond (100) (2 × 1) surface results in an even greater NEA of -3.50 eV for 1 ML.

Other alkali metals, such as sodium, potassium and caesium, have all been investigated using DFT calculations. Although the results suggest they all induce a true NEA on the diamond surface, they are all of a smaller magnitude in comparison to lithium. The calculations revealed that they had much lower adsorption energies, and in the case of potassium and caesium a full monolayer is not possible<sup>[60]</sup>.

Magnesium is also a promising choice. Adsorption onto oxygen-terminated diamond (100) at 0.5 ML coverage displayed an NEA of -2.01 eV and a work function of 2.40 eV<sup>[61]</sup>. This suggests that magnesium and lithium are the most viable options for practical applications which require a large NEA and the surface to be stable.

## 1.5 – Analysis of Terminated Diamond Surfaces

### 1.5.1 – Wettability

The surface of a material often governs its physical properties. Due to this, surface interfaces are important for analysis of materials. One property that can be looked at is surface wetting. The degree of wetting is due to the intermolecular interactions between the liquid, a solid surface, and the gaseous environment. These interactions can be split into two main categories, cohesive forces and adhesive forces. Cohesive forces are the interactions that favour the attraction of like molecules, in this case the liquid. Adhesive forces are the interactions that favour attraction at the phase interface between the liquid and the solid. If the liquid and gas used remains constant, then only the adhesive interactions need be considered.

When a small drop of liquid is deposited onto the surface of a solid, an isolated drop forms. The contact angle of the deposited drop with the solid surface is an indicator of the adhesive forces. The contact angle ( $\theta$ ) must satisfy the inequality  $0 \leq \theta \leq 180^\circ$ , where  $\theta = 0^\circ$  corresponds to no wetting, and  $\theta = 180^\circ$  corresponds to full wetting. These are both extreme examples. Generally instead, the terms wetting and non-wetting are used for  $\theta < 90^\circ$  and  $\theta > 90^\circ$ , respectively. If investigating the interaction between water and a surface, a non-wetting surface is characterised as hydrophobic and a wetting surface characterised as hydrophilic<sup>[62]</sup>. This method for studying interfacial interactions is known as the sessile drop method and is shown in Fig. 14.

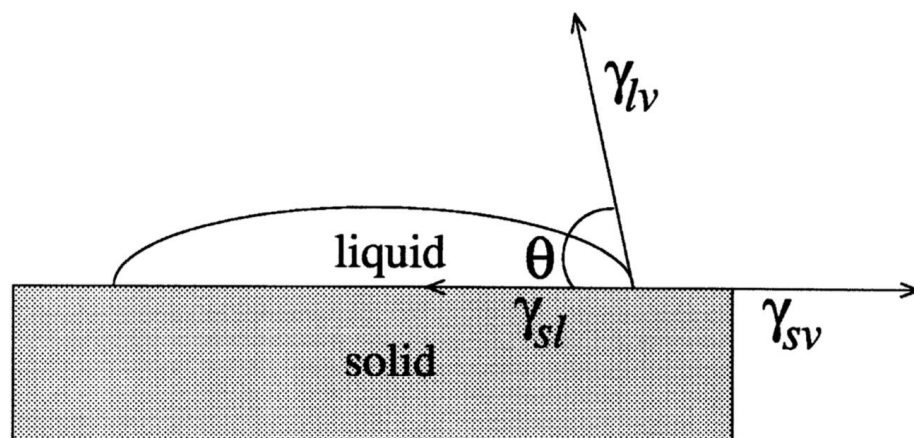


**Figure 14: A diagram showing how the contact angle,  $\theta$ , is measured using the sessile drop method. The contact angle is defined by the three phase interfaces; solid-vapour ( $\gamma_{sv}$ ), solid-liquid ( $\gamma_{sl}$ ), and liquid-vapour ( $\gamma_{lv}$ ).<sup>[63]</sup>**

These interfacial tensions can be related to the contact angle by the Young's equation:

$$\gamma_{lv} \cdot \cos\theta = \gamma_{sv} - \gamma_{sl} \quad (\text{Eq. 3})$$

where  $\gamma_{sv}$ ,  $\gamma_{sl}$ , and  $\gamma_{lv}$  are the solid-vapour, solid-liquid and liquid-vapour interfaces, respectively. If the only variable of the three phases is the solid, then  $\gamma_{lv}$  can be considered constant. If the solid-vapour interfacial tension is greater than that of the solid-liquid ( $\gamma_{sv} > \gamma_{sl}$ ),  $\cos\theta$  will be positive. Therefore, the contact angle will be greater than  $90^\circ$ , indicating a wetting interaction. The opposite is true if the solid-liquid interaction is less favourable than the solid-vapour interaction<sup>[62]</sup>.

Previous research into the wettability of the diamond surface shows a distinct change in wettability with changing surface termination. Hydrogen-termination of the diamond surface results in a hydrophobic surface ( $\theta = 93^\circ$ )<sup>[64]</sup>. Fluorinated diamond surface is similarly hydrophobic ( $\theta = 93^\circ$ )<sup>[19]</sup>. In contrast, the oxygen-terminated diamond surface is hydrophilic, for which Mertens *et al* reported a contact angle measurement of  $42.3 - 51.4^\circ$ <sup>[65]</sup>.

### 1.5.2 - Surface Roughness

Different methods and conditions used for CVD diamond growth produce varying film structures. CVD diamond films contain the (100), (111) and the (110) surface structure. However, depending on conditions and methods, different ratios of each can be obtained and in varying facet magnitude. This results in surface roughness, which in turn affects the coverage of the terminating atoms. Surface roughness also poses a problem for many analytical techniques. Water contact angle measurements require a clean and smooth surface. Small cracks or scratches in the surface can vastly affect the recorded contact angle. CVD methods are capable of growing three main varieties of diamond, all differing in structure and surface quality. In order of decreasing surface roughness, these are polycrystalline, nanocrystalline and single crystal. The diamond film samples grown in this project are all polycrystalline, and therefore have a rough surface structure. The effect of surface roughness on contact angle was described by Wenzel using the below equation;

$$\cos\theta_{app} = R_{rough} \cdot \cos\theta_y \quad (\text{Eq. 4})$$

Here,  $\theta_{app}$  is the contact angle that is experimentally observed or the apparent contact angle.  $R_{rough}$  is a ratio between the actual surface area and the geometric surface area of the solid.  $\theta_y$  represents the contact angle in the absence of surface roughness, or Young contact angle. If the surface is atomically smooth, then  $R_{rough}$  is equal to one, and  $\theta_{app}$  will be equal to  $\theta_y$ . Values for  $R_{rough} > 1$  indicate surface roughness. This equation implies that for hydrophobic surfaces ( $\theta > 90^\circ$ ), roughening of the surface will increase hydrophobicity. For hydrophilic surfaces ( $\theta < 90^\circ$ ), surface roughness will increase hydrophilicity<sup>[62]</sup>.

## **2. – Material Preparation and Experimental Techniques**

---

### **2.1 – Project Aim**

There were three principle aims to this project. The first was to successfully grow polycrystalline diamond using the hot filament (HF) CVD method. The second was to modify a custom-built DC plasma termination (DCPT) reactor to allow heating of diamond substrates. The final objective was to utilise the newly customised DCPT reactor to investigate the effect that heating of the diamond substrate has on efficacy of hydrogen and oxygen surface termination. Results were characterised using analytical techniques, such as contact angle measurements, Raman spectroscopy, and scanning electron microscopy (SEM).

### **2.2 – Preparation of CVD diamond Samples**

As mentioned, the initial stage of this project involved the growth of polycrystalline diamond samples to be used in further experiments involving termination of the diamond surface.

#### **2.2.1 – Preparation of Substrate**

N-type silicon wafer was used as a substrate for heteroepitaxial CVD diamond growth. The samples used were 1 × 1 cm in size, with a polished and unpolished side. The samples had the (100) surface structure. For heteroepitaxially grown CVD diamond, initial growth is very slow, unless the silicon is pre-treated to provide nucleation sites. To achieve this, the polished side was subjected to manual abrasion using microcrystalline diamond powder. This resulted in a layer of diamond debris and scratches in the silicon wafer, which aids the growth of an sp<sup>3</sup> hybridised lattice. Samples were then gently cleaned using ethanol to remove bulk quantities of powder.

#### **2.2.2 – Hot Filament CVD Reactor**

All samples were grown using a HFCVD reactor. The structure of the reactor can be broken down into three parts; reaction chamber, gas feed and gas removal. A detailed schematic diagram of this is shown in Fig. 15. Gases were stored in gas cylinders located in a separate room as a safety precaution. Methane and hydrogen were delivered to mass flow controllers (MFCs) via stainless steel pipes. The MFCs allowed the flow of the methane and hydrogen to be set at a desired rate and ratio. Following the MFCs, the gases were fed to the reaction

chamber through the gas inlet, via a further stainless steel pipe. Waste gas was removed with aid from a rotary vacuum pump (Leybold, Trivac D8B) located below the reaction chamber. In between the reaction chamber and the vacuum pump were three valves, which allowed control over the removal of waste gas.

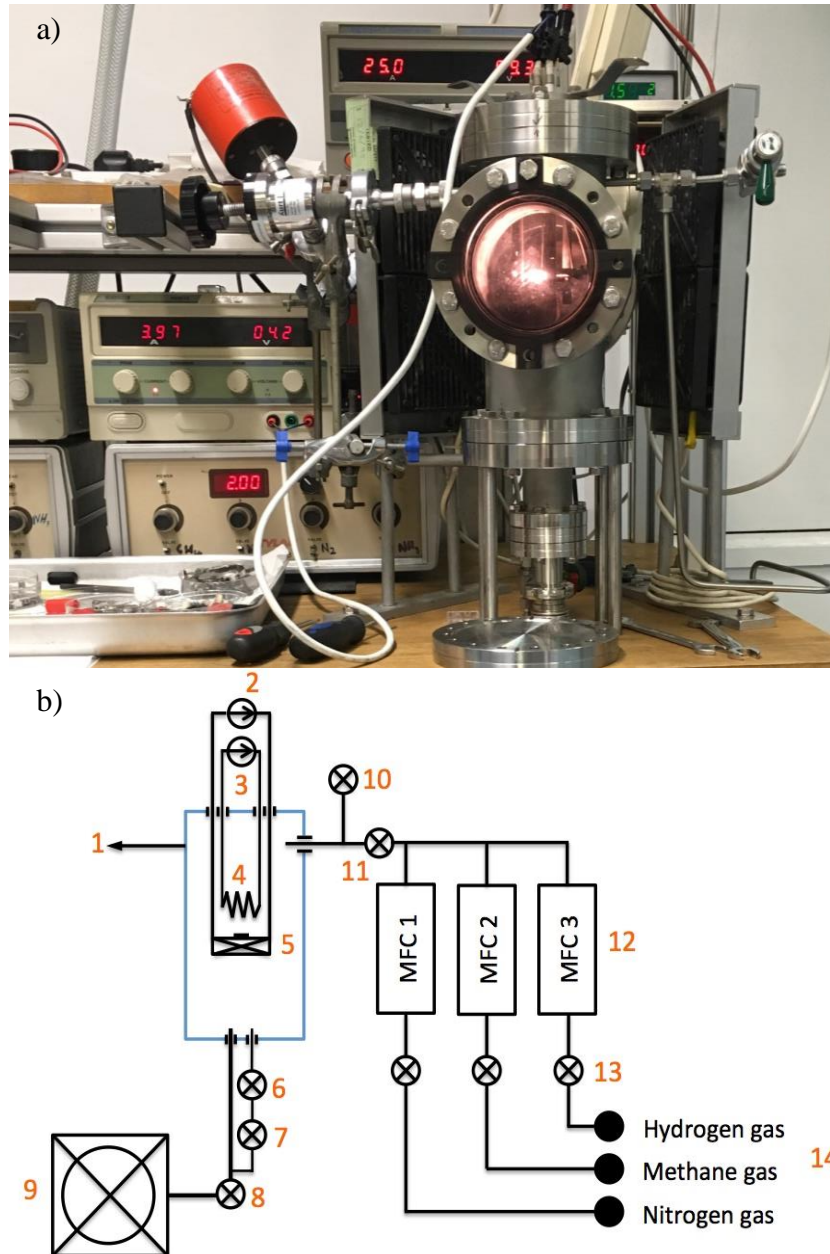


**Figure 15: Photograph of the HFCVD reaction chamber (a). Schematic diagram of the HFCVD reactor (b). Components are as follows; 1 – gas line to pressure gauges, 2 – filament power supply, 3 – heater power supply, 4 – tantalum filaments, 5 – sample holder/ heater, 6 – needle valve, 7 – butterfly valve, 8 – shutoff valve, 9 – rotary vacuum pump, 10 – vent, 11 – main gas inlet valve, 12 – mass flow controllers, 13 – individual gas inlet valves, 14 – gas cylinders<sup>[66]</sup>.**

The reaction chamber was constructed of stainless steel and contained a removable holder, upon which the silicon substrate resided during CVD growth. The sample holder was made of molybdenum and was electrically resistance heated using a DC bench power supply (HQ PS3010), passing 4 A current through embedded heater wires. The sample holder was capable of holding two  $1 \times 1$  cm samples. A few millimetres above this surface were three tantalum filaments in which 25 A power was supplied using a Digimess (SM3040). The tantalum filaments were replaced after each growth run. On replacing the filaments, the wire was pulled taut and clamped at both ends. One end of each filament was fixed in place with a spring loaded clamp. This was to allow for expansion and contraction of the filaments that occurred during heating and cooling. It was paramount that the filaments were taut before clamping to ensure the filaments were always an even distance from the substrate. The sample holder and filament setup can be seen in Fig. 16.

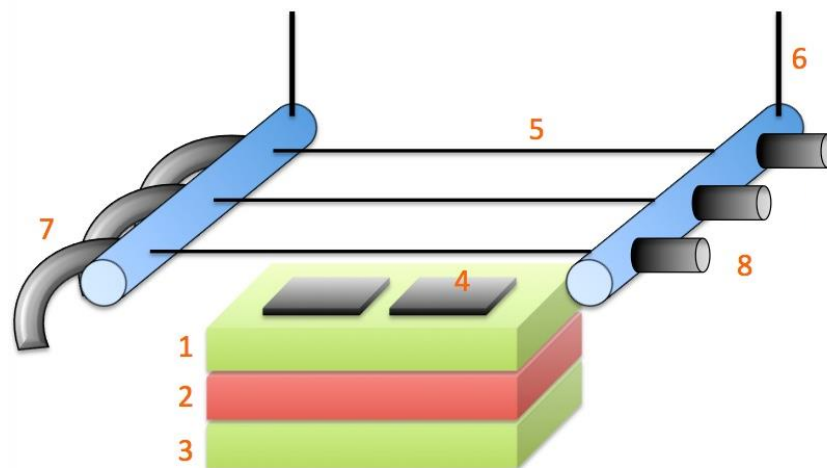


**Figure 16: Diagram of the filament assembly within the HFCVD reaction chamber. The components are as follows; 1 – molybdenum substrate plinth top, 2 – substrate heater, 3 – stainless steel substrate holder bottom, 4 – substrate, 5 – tantalum filaments, 6 – filament power connection, 7 – spring loaded filament clamp, 8 – filament clamp<sup>[66]</sup>.**

Pressure in the reaction chamber was adjusted using the needle valve located between the reaction chamber and the vacuum pump. The pressure was monitored using two separate pressure gauges. A Pirani (Edwards, PG100-XM) was utilised for the lower pressures, to allow monitoring of the base pressure. Monitoring of the higher pressure used during CVD growth was achieved using a capacitance manometer (Vacuum General, CMLB-21).

### **2.2.2.1 – Standard Operating Procedure**

All samples were grown using the same method. The tantalum filaments were replaced at the beginning of each CVD diamond growth run. Two silicon wafers, pre-treated as previously mentioned, were placed on the sample holder. The reaction chamber lid and the attached sample holder was placed on top of the reactor. A rubber O-ring was present between the lid and the reaction chamber to ensure an airtight seal. The lid was then secured with bolts prior to CVD growth. The air vent was then closed, and the reaction chamber pumped down until a base pressure of  $<50 \times 10^{-3}$  Torr was established. Current was then supplied to the substrate heater (4.0 A). This was maintained for 30 minutes, prior to supplying reaction gases to the reaction chamber. To do this, the MFCs for both hydrogen and methane were turned on. The rates for hydrogen and methane were set at 200 standard cubic centimetres per minute (sccm) and 2 sccm respectively, providing a 1:100 H<sub>2</sub>:CH<sub>4</sub>. The pressure in the reaction chamber was adjusted to 20.0 Torr using the needle valve connected to the vacuum pump. Once the pressure within the reaction chamber had been stabilised at 20.0 Torr, the power supply for the filaments was switched on. The current applied across the filaments was a constant 25 A. This was maintained for 3 hours, resulting in a polycrystalline diamond film forming on the silicon substrate. The resultant diamond layer was approximately 1  $\mu\text{m}$  thick.

### **2.2.3 – Hydrogen Termination Using the Microwave Plasma Reactor**

The CVD samples were synthesised at varying times throughout the project. While waiting in ambient air to be analysed or further processed, the diamond films were exposed to atmospheric oxygen, which can displace surface hydrogen atoms over time. Due to this, the samples would have varying surface composition. To counteract this effect, all samples were re-hydrogen-terminated using a microwave CVD (MWCVD) reactor immediately prior to experiments involving the DCPT reactor. This ensured that all samples had identical surface composition.

The MW reaction chamber was stainless steel and cooled using water. Gases were supplied to the reaction chamber via stainless steel pipes. The gases were exposed to microwave radiation created by the magnetron (1.5 kW, 2.45 GHz, Seki-ASTeX microwave generator). The gases were excited and formed a plasma, located above the diamond sample. All hydrogen terminations were executed using the same conditions. These are as follows; a base pressure of

$2.0 \times 10^{-3}$  Torr was established before hydrogen was introduced, raising the pressure to 30 Torr. In order to strike the plasma, 650 W was supplied to the magnetron. Once a plasma was established, the pressure was raised to 80 Torr and the power raised to 1150 W, resulting in a substrate temperature of  $\sim 900$  °C (measured using a single-coloured optical pyrometer). This was maintained for 2 minutes before lowering the pressure and power to 30 Torr and 650 W respectively, resulting in a substrate temperature of  $\sim 500$  °C. Again this was maintained for 2 minutes. The power was then changed to 0 W, terminating the plasma. This final stage lasted for 2 minutes and was to allow the sample to cool to room temperature whilst being subjected to hydrogen gas. In doing this, the hydrogen on the surface of the diamond film was less likely to desorb when exposed to air.

By performing these hydrogen terminations on the surface, the samples would have been cleaned of impurities and, in theory, should all have a full hydrogen surface termination.

### **2.3 – DC Plasma Termination Reactor**

The reactor used for performing the further terminations on the CVD diamond films was repurposed from a sputter coater (Edwards, S150A). Sputtering occurs when a target material is bombarded with high energy particles, usually ions, causing atoms to be removed from the material. The creation of the ions is achieved by applying a strong current between an anode and cathode across a neutral gas in order to generate a plasma. In the modified version of the reactor, this generated plasma is used to alter the composition of the diamond termination.

Prior to this project, the sputter coater was modified to include gas feed and removal. A full schematic diagram of the DCPT is shown in Fig. 17. As with the HFCVD reactor, for safety precautions, the gases were stored in gas canisters that reside in a neighbouring room. The gases were then fed via stainless steel pipes to multiple MFCs. Currently there are three gas lines, these facilitate the flow of hydrogen, oxygen and nitrogen. The nitrogen line could be switched over to allow use of other gases, such as SF<sub>6</sub> and ammonia. The gas flows were set to 10 sccm. Subsequently, further stainless steel pipes supplied the gas to the DCPT reactor chamber, via a gas mixer and gas inlet valve. The gas output was connected to a rotary vacuum pump (Leybold, Trivac D10E), facilitating removal of waste gas and maintaining the low pressures required for plasma formation. The reaction chamber pressure was monitored using two pressure gauges. The Leybold (Thermovac, TM 20) measured a range of pressures in the

chamber, from atmospheric to mTorr. This was utilised for identifying the base pressure. A capacitance manometer (Baratron) is a more accurate pressure gauge, and was used to monitor the pressure used during terminations (1.0 Torr). The pressure in the chamber was adjusted using a valve attached to the rotary vacuum pump.

Utilising this reactor, multiple terminations using different gases have been attempted. These are oxygen, hydrogen, fluorine, nitrogen and ammonia terminations, using O<sub>2</sub>, H<sub>2</sub>, SF<sub>6</sub>, N<sub>2</sub>, NH<sub>3</sub> gases respectively. Of these terminations, oxygen, fluorine and ammonia were reported to be the most successful<sup>[66],[67]</sup>. The hydrogen termination only resulted in partial coverage of the diamond surface, and termination using nitrogen gas proved to be completely unsuccessful. In order to improve the efficacy of termination using H<sub>2</sub> and N<sub>2</sub> gas, the reactor was modified to include a substrate heating system.

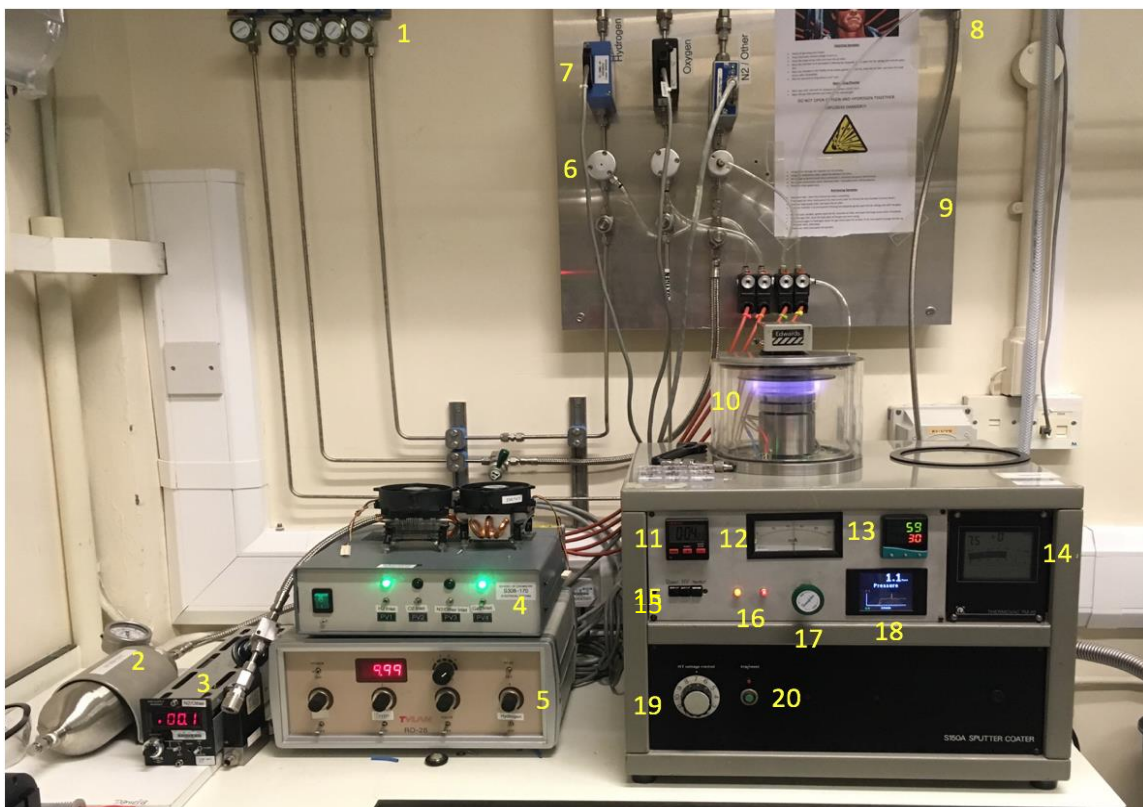


**Figure 17: Photograph of the complete set-up for the DCPT reactor. Components labelled as follows; 1 – wall gas valves, 2 – substitutable gas canister, 3 – N<sub>2</sub>/other MFC controls, 4 – pneumatic gas valve controls, 5 – H<sub>2</sub>/O<sub>2</sub> MFC controls, 6 – pneumatic gas valves, 7 – gas MFCs, 8 – pneumatic gas inlet valve, 9 – gas inlet pipe, 10 – reaction chamber, 11 – plasma timer, 12 – amp meter, 13 – temperature controller, 14 – base pressure gauge, 15 – heater/power/plasma switches, 16 – plasma/power indicator lights, 17 – air inlet valve, 18 – operating pressure gauge, 19 – plasma power dial, 20 – plasma trip switch.**

### 2.3.1 – Modifications

To aid effective termination, a system for heating the substrate was installed in the DCPT reactor. To achieve this, two holes were drilled within the stainless steel anode, on which the diamond film resides. These cavities allowed two cartridge heaters (Watlow, FIREROD) to be embedded into the plate. A small hole was drilled in the centre of the anode, directly below the substrate position. A thermocouple was inserted into the cavity, allowing monitoring of the substrate temperature. The hole was drilled a corresponding size to the thermocouple, guaranteeing direct contact between the thermocouple and the anode. Contact between the anode and the thermocouple was imperative for ensuring accurate temperature readings. The modifications can be seen in Fig. 18b.

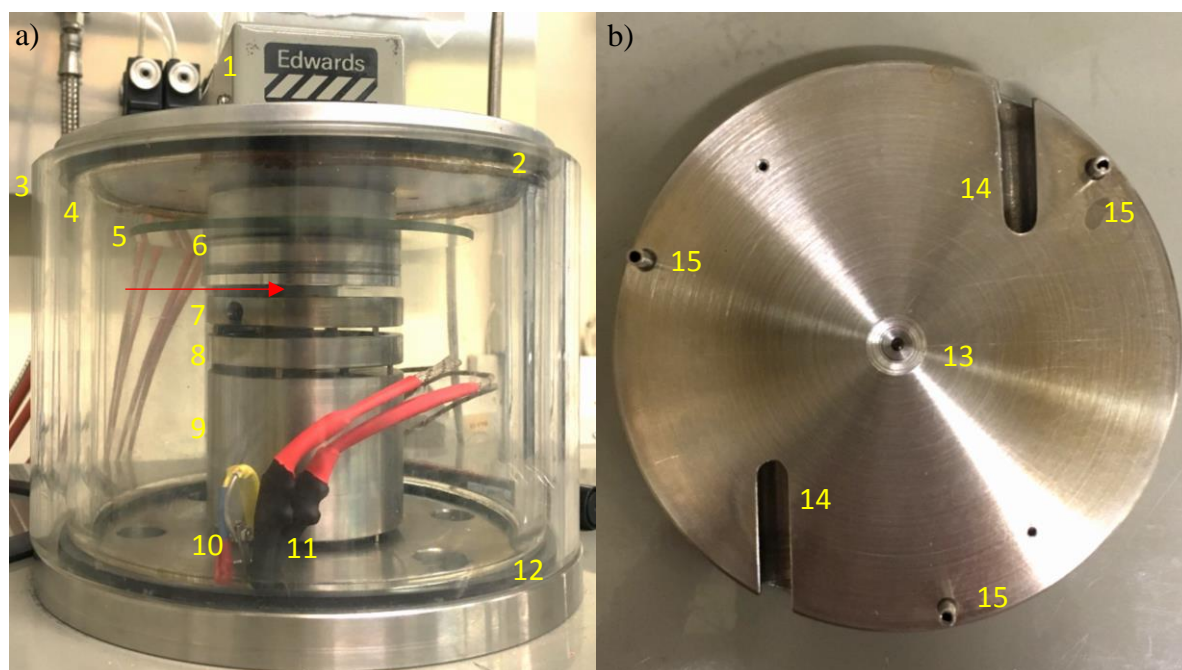


**Figure 18: Photograph of the reaction chamber (a). Components listed as follows; 1 – plasma power supply, 2 – upper rubber O-ring, 3 – plastic protective shield, 4 – glass chamber, 5 – plasma shield, 6 – cathode, 7 – anode (sample holder), 8 – tower layer, 9 – tower base, 10 – thermocouple connection, 11 – heating cartridge connection, 12 – lower rubber O-ring. The red arrow indicates where the sample resided and the plasma formed. Image (b) shows a photograph of the anode (underneath side). 13 – hole for thermocouple, 14 – holes for heater cartridges, 15 – metal pins for elevation.**

Both the thermocouple and heaters were wired to a temperature controller (TC) (CAL 9400), which is mounted to the control panel on the reactor. The TC translated the electrical output from the thermocouple into a temperature, so the substrate temperature could be continuously monitored. The desired temperature could be set using a pre-existing function available on the

TC. When this function was engaged, the TC monitored the temperature using the thermocouple and then adjusted the output to the heaters accordingly, until the set temperature was reached. It would then maintain the desired temperature until the set temperature was altered. However, a switch was wired between the TC and the heaters to allow the heaters to be quickly engaged or disengaged.

In the original design of the reaction chamber, the anode was elevated by a copper pedestal. However, copper has a high thermal conductivity and would facilitate the dispersion of heat from the anode other areas of the reactor. To effectively heat the anode to high temperatures, minimal heat dispersion is optimal. For this reason, the copper pedestal was removed and replaced with a layered tower model (Fig. 18a). The layered tower model consisted of the anode, with two further stainless steel layers below. Between each layer, were three small pins elevating the above layer. The small area of contact between the layers drastically decreased the heat dispersion from the anode to the rest of the reactor. In the new model, the majority of heat dispersion should occur via the gaseous atmosphere, which at the operating pressure of 1.0 Torr, would be negligible.

### **2.3.2 – Heater Calibration**

The temperature controller required calibration in order to better maintain the set point temperature. Data were recorded to display temperature as a function of time so that the effectiveness of the calibration could be quantified (Fig. 19). All tests were run under termination conditions (1.0 Torr, O<sub>2</sub> or H<sub>2</sub> atmosphere), in order to correctly calibrate the temperature controller. A temperature set point of 100 °C was used for all tests, as this was the minimum temperature at which the TC is capable of calibration.

Prior to calibration, the temperature exceeded the set point by ~25 °C. Furthermore, the TC reengaged the heaters once the temperature cooled to ~110 °C, resulting in the temperature returning to ~125 °C. The temperature continued to fluctuate, never reaching the set temperature. Calibration of the temperature controller seemed to alleviate some of these issues. Initial heating would only result in a temperature of 114 °C. The large fluctuations in temperature were eliminated, and the temperature remained much closer to the set temperature (100 °C). Further monitoring of the temperature (not displayed in Fig. 19) revealed the

temperature was at 102 °C after 30 minutes of the heater being powered. A similar test completed in a hydrogen atmosphere, rather than oxygen, showed some improvements in comparison to pre-calibration. The temperature fluctuations are still noticeable, but are only 3-5 °C. This is a considerable improvement from the 10-15 °C fluctuations prior to calibration. Again, after 30 minutes, a temperature of 102 °C was reached.

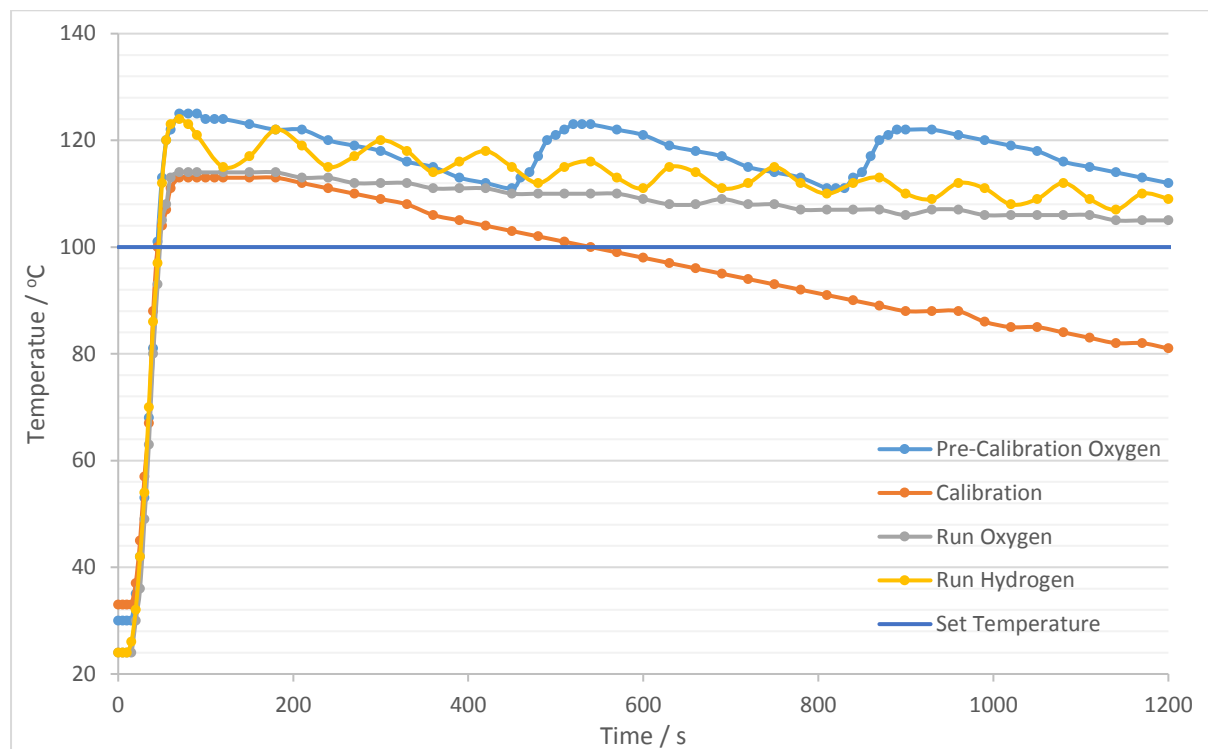


**Figure 19: Temperature of the heating elements within the DC plasma reactor as a function of time, whilst the set point is 100 °C. The blue plot is prior to calibration of the temperature controller. The grey and yellow plots are post-calibration.**

### 2.3.3 – Standard Operating Procedure

Throughout the project, all terminations using DCPT reactor were executed using the same standard operating procedure, bar a few variants. These variants were the reaction gas, temperature, and plasma duration.

The CVD diamond sample was placed in the centre of the anode before closing the reaction chamber, ensuring the rubber O-ring was aligned. The air inlet was closed, and the main valve for the vacuum pump opened, providing an airtight seal of the reaction chamber. The pressure was allowed to decrease until a base pressure of  $2.0 \times 10^{-2}$  Torr was reached. The wall valve,

and pneumatic valve for the desired termination gas were opened. The MFC for the gas was then turned on, allowing continuous flow of the termination gas (10 sccm). Finally, the pneumatic gas inlet valve was opened to allow the gas to flow into the reaction chamber. To ensure any impurities in the chamber were removed before termination, the reactant gas flowed through the chamber for 10 minutes, whilst the vacuum pump was still engaged. The pressure was then adjusted using the needle valve on the vacuum pump until a pressure of 1.0 Torr was reached. If heating of the sample was required, then the heaters would be engaged now after setting the TC to the desired temperature. Once the set temperature was reached, the voltage dial was set to 7 (corresponding to 48 mA current) and the required plasma duration was set on the timer. Starting the timer initiated plasma generation. Once the plasma ceased, the heaters were turned off and the voltage was returned to 0 V. The gas inlet valve was then closed and the needle valve on the vacuum pump opened. The reactor was left for 15 minutes to allow all residual gases to be removed from the chamber. The main vacuum valve was then opened, and the air inlet valve was slowly opened until atmospheric pressure was reached, before opening of the chamber and removal of the samples.

## **2.4 – Analysis of the Terminated Surface**

### **2.4.1 – Contact Angle Measurements**

Due to the ease and effectiveness of the sessile drop method, water contact angle measurements were performed frequently throughout the project to characterise the diamond surface. As previously mentioned, the hydrogen and oxygen-terminated diamond surface is hydrophobic and hydrophilic, respectively. Therefore, using the water contact angle measurements, the degree of hydrogen or oxygen termination could be qualitatively assessed. All contact angles were measured using the Krüss drop shape analyser (DSA) 100 (Fig. 20), coupled with the Krüss program, Advance.

A pipette was manually filled with deionised water, prior to insertion into the DSA. A droplet, of size 1.5  $\mu\text{L}$ , was measured and deposited onto the sample by the automated system built into the DSA. A live image of the water droplet gives the contact angle in real time. The program provided surface contact angle measurements for both the left and the right hand side of the water droplet. This was done twice for each sample. An average of all four angles was

calculated. Before contact angle measurements were recorded, the drop was allowed exactly 3 s to equilibrate, ensuring consistent results.

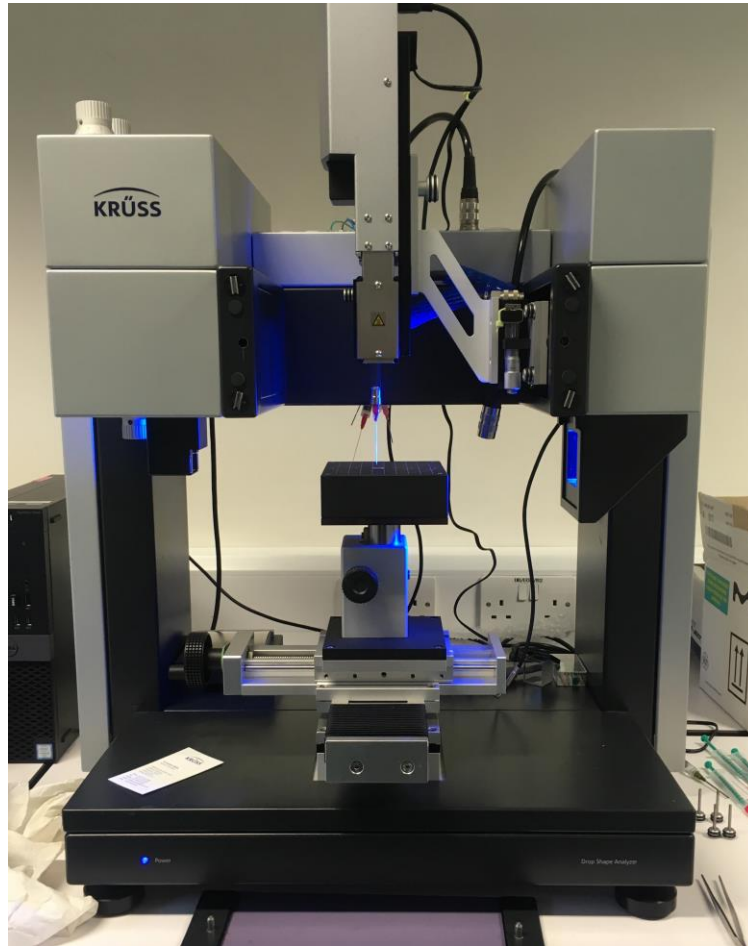


**Figure 20: The Krüss drop shape analyser (DSA) 100, which paired with Advance, was used to measure all recorded water contact angle measurements.**

### 3. – Results and Discussion

---

#### 3.1 – Scanning Electron Microscopy

Scanning electron microscopy (SEM) is a useful method to confirm CVD diamond growth and examine the quality of the diamond created. However, SEM is unable to characterise the atomic composition of the diamond film itself, such as graphitic character or the identity of the terminating atoms.

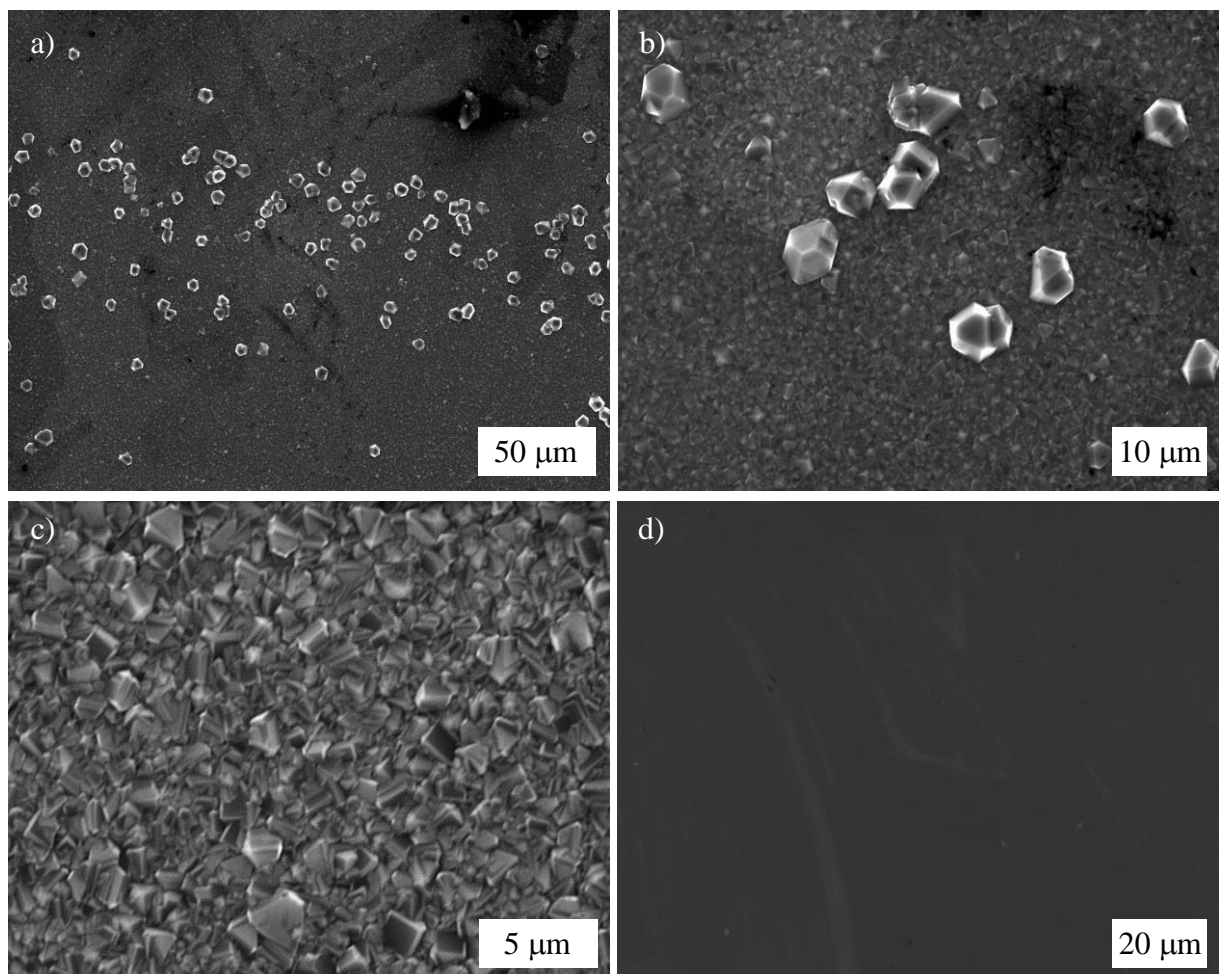


**Figure 21: SEM images of CVD diamond film grown in the non-boron-doped HF Reactor. (a)  $\times 500$  zoom of CVD diamond film, showing a row of larger crystals within the diamond film, likely due to the use of manual abrasion techniques (b)  $\times 2000$  zoom of CVD diamond film. A closer examination of the larger diamond facets within the more uniform polycrystalline film (c)  $\times 5000$  zoom of CVD diamond film. Shows the bulk formation of the polycrystalline diamond film (d)  $\times 1000$  zoom of the Si 100 surface prior to CVD diamond growth.**

All of the images were taken in the University of Bristol Chemical Imaging Facility, using a Jeol IT300 SEM, operating at 15kV. Images of the CVD diamond film at varying magnification are shown in Fig. 21a to 21c. For reference, the n-type silicon wafer used as a base for CVD growth is shown in image Fig. 21d. From comparison of the images, it is clear that CVD diamond growth has taken place, forming a polycrystalline diamond film. Prior to growth in the HFCVD reactor, the silicon wafers were manually abraded with microcrystalline diamond powder. This was employed to create nucleation sites which aid CVD diamond growth. In images (a) and (b), larger sporadic facets are visible within the bulk diamond structure. This is likely due to using manual abrasion, which can lead to uneven nucleation of the silicon substrate, and therefore uneven diamond growth. Image (c) shows the bulk crystalline structure of the diamond film. The diamond facets here are more uniform in size.

### 3.2 – Laser Raman Spectroscopy

Laser Raman spectroscopy was utilised to confirm successful synthesis diamond films grown using the HFCVD reactor. All spectra were taken using the Renishaw 2000 spectrometer, coupled with a 514 nm laser (Green, Ar<sup>+</sup>).

The Raman spectrum of crystalline diamond results in a sharp first order peak at 1332 cm<sup>-1</sup> and can therefore be used as a clear indication of effective diamond formation. Raman spectroscopy is also useful in gauging the quality of the diamond produced, by highlighting any graphitic character within the film. Crystalline graphite results in a peak at 1580 cm<sup>-1</sup>, and amorphous graphite contributes to a broad G-band between 1520-1580 cm<sup>-1</sup>[68].

Laser Raman spectroscopy was used to analyse the Si substrate, and three visibly varying structures within the CVD diamond film (Fig. 22). The spectra of all four surfaces are displayed in Fig. 21. The spectra have been separated for clarity. All three spectra of the CVD diamond film displayed a sharp first order peak at 1334 cm<sup>-1</sup>, indicating diamond formation. The three spectra also contain a broad G-band between 1500 and 1650 cm<sup>-1</sup>. This suggests considerable graphitic character in the diamond film. Although much less intense, the silicon peak between 920 and 1000 cm<sup>-1</sup> is still present in the spectra of the CVD diamond film. This is likely due the laser penetrating the thin film diamond, to the silicon wafer below.

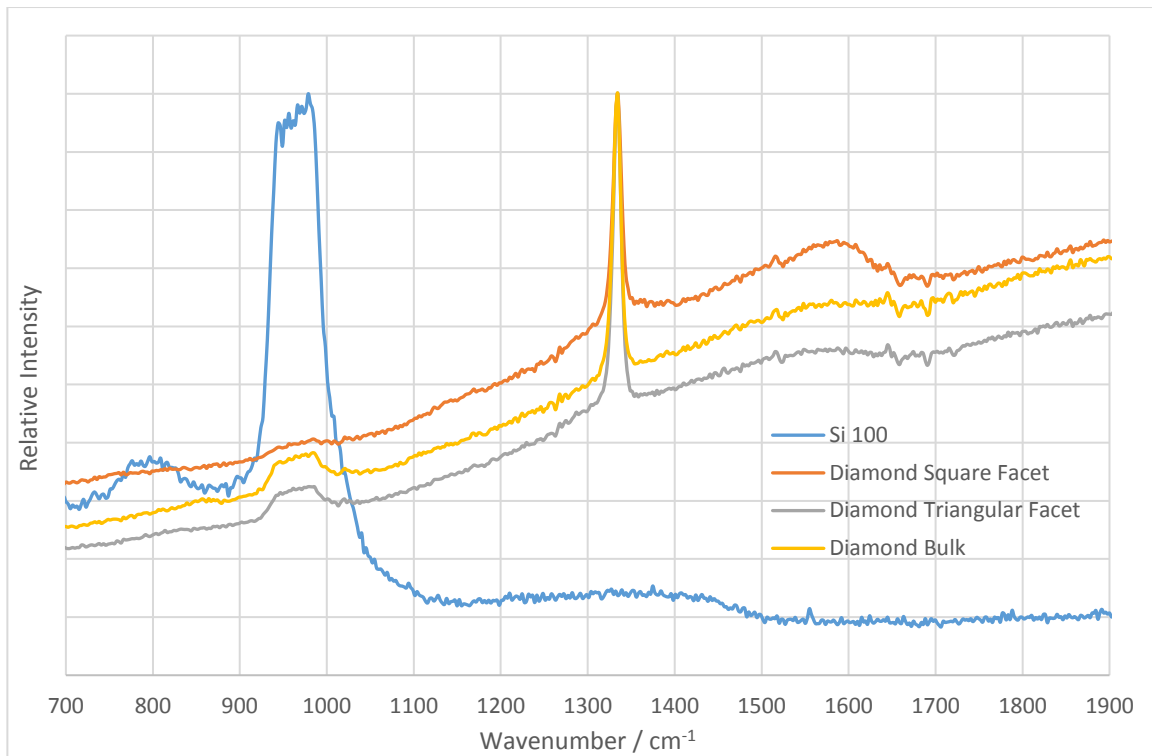


**Figure 22: Laser Raman spectra from CVD diamond film, grown using HF reactor. Spectra were recorded at three different locations on the diamond film; square facet, triangular facet and bulk. A final spectrum was recorded for reference, of the Si 100 wafer used as a base for CVD growth.**

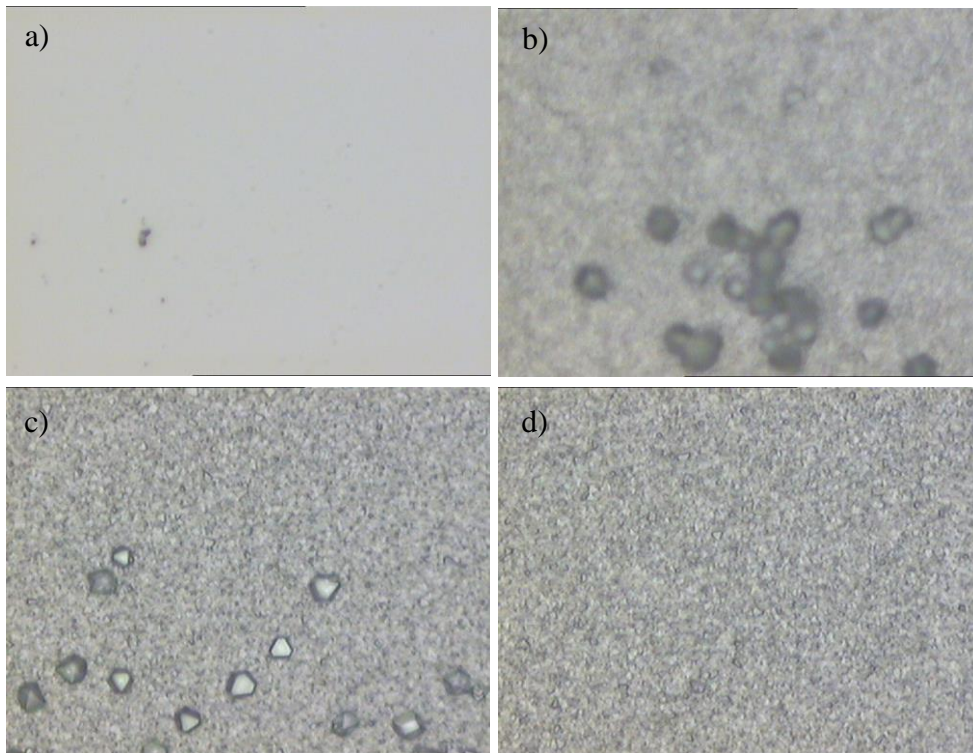


**Figure 23: Images of the four surfaces which were analysed using laser Raman spectroscopy. (a) silicon substrate (b) CVD diamond square facet (c) CVD diamond triangular facet (d) bulk CVD diamond.**

### 3.3 – Contact Angle Measurements

#### 3.3.1 – Oxygen Termination

Previous research had been completed regarding oxygen termination of the diamond film surface using the DCPT reactor. Exposure of the diamond surface to oxygen plasma for 5 to 8 s at room temperature was found to result in the highest oxygen surface coverage. Longer oxygen plasma caused etching of the surface and resulted in a lower oxygen coverage<sup>[66]</sup>. However, this was prior to installation of the substrate heaters, so temperature could not be varied. Since these results, the reactor has been heavily modified. Because of this, oxygen termination using the DCPT reactor was re-examined.

Three different plasma times were chosen, based on previous studies (4 s, 7 s, 10 s). Two samples were also heated whilst oxygen terminated. A lower plasma time (4 s) was used. The lower plasma time was used as previous studies found that, at room temperature, a 4 s plasma duration did not result in a full oxygen coverage. Therefore, the effect of heating would hopefully be more visible. Prior to the oxygen termination, the polycrystalline samples were hydrogen terminated using the MWCVD reactor.

**Table 2: Conditions used for oxygen termination of CVD diamond using the DCPT reactor, and the resulting average water contact angle measurements.**

Sample	Termination	Plasma Time / s	Temperature / °C	Average Contact Angle ( $\theta$ ) / °	Standard Deviation ( $\sigma$ )
1	Hydrogen	N/A	N/A	98.9	4.5
2	Oxygen	4	24	57.8	2.5
3	Oxygen	7	24	48.0	1.6
4	Oxygen	10	25	61.7	4.0
5	Oxygen	4	65	61.7	0.7
6	Oxygen	4	125	65.4	1.4

The resultant average contact angles for each termination are shown in Table 2. Sample 1 was hydrogen terminated using the MWCVD reactor. Ostrovskaya reported a water contact angle of 93° for hydrogen-terminated polycrystalline diamond film<sup>[64]</sup>. This is in close agreement with the resultant contact angle for sample 1 ( $98.9^\circ \pm 4.5^\circ$ )

Literature values for oxygen-terminated diamond films vary substantially depending on the film structure. Mertens *et al* reported a contact angle of  $42.3 - 51.4^\circ$  for oxygen-terminated nanocrystalline diamond film, grown using the HFCVD method<sup>[65]</sup>. This value is in close agreement with the resultant contact angle for oxygen-terminated sample 3 (7 s, room temperature,  $48.0^\circ \pm 1.6^\circ$ ). As mentioned earlier, previous work using the DCPT reactor also found the ideal conditions to be a plasma duration between 5 and 8 s at room temperature<sup>[66]</sup>.

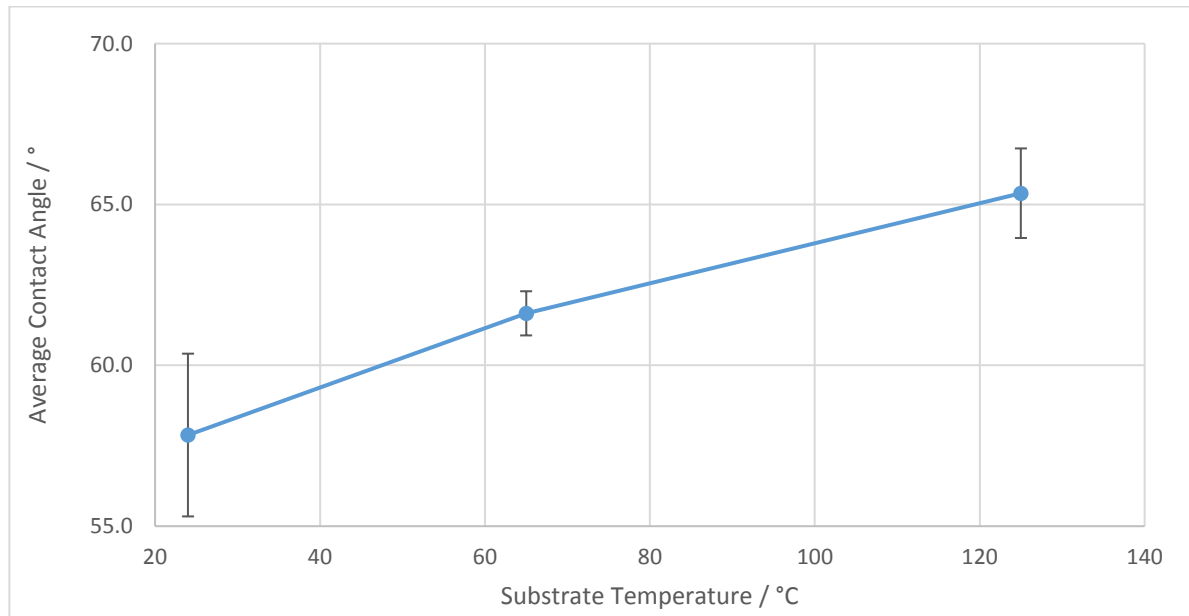


**Figure 24: Graph showing the effect of substrate temperature on oxygen termination of polycrystalline diamond films achieved using an oxygen plasma time of 4 s.**

Using the substrate heating system installed, the effect of substrate temperature on efficacy of oxygen termination was explored. An oxygen plasma time of 4 s was used, at three different temperatures. The results are shown in Fig. 24. Interestingly, the hydrophilicity of the diamond films decreases with increasing temperature. This indicates a decrease in efficacy of oxygen termination. The contact angle measurements varied depending on the locality of the water droplet on the terminated film. This is reflected in the uncertainty, which was obtained by calculating the standard deviation of the angles.

An image from the drop shape analyser is shown in Fig. 25. The droplet is situated on the most hydrophilic diamond sample obtained from the above terminations (7 s, room temperature). Once the drop is placed on the diamond surface, it is left to stabilise for 3 s before the contact angle measurements are taken. As only a small drop is deposited on the surface, the contact angles continuously change due to evaporation of the droplet. The image shown in Fig. 25 was

taken roughly 10 s after the drop was deposited on the film, resulting in a higher contact angle value in comparison to the value recorded (48.0°).

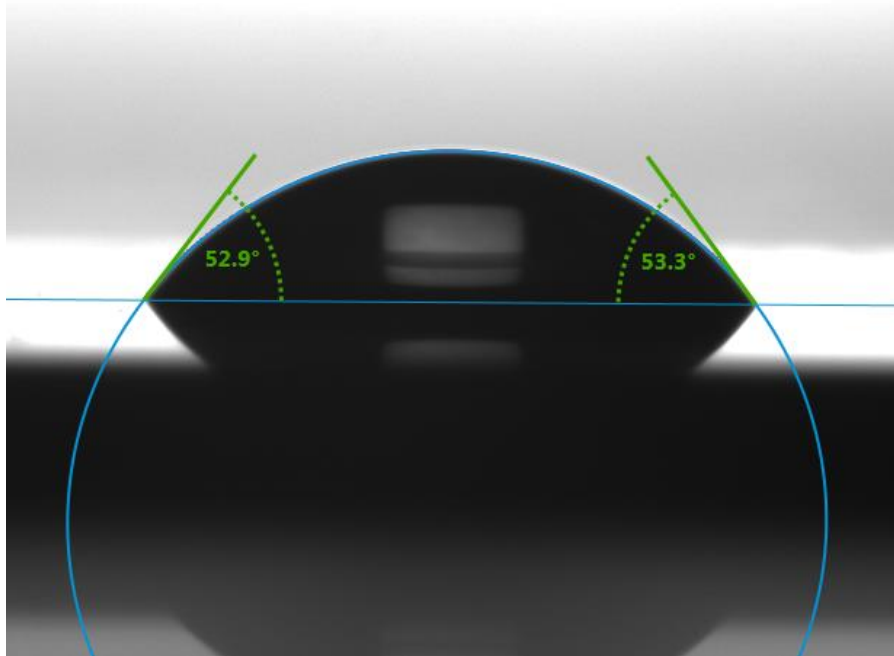


**Figure 25: Image of a 1.5  $\mu\text{L}$  water droplet on the oxygen-terminated surface. The conditions used for this oxygen termination were a plasma duration of 7 s, and temperature of 24 °C. Image taken using the Krüss DSA, in conjunction with the Advance program.**

### 3.3.2 – Hydrogen Termination

Five different temperatures were chosen for hydrogen termination. The temperatures investigated were confined to 200 °C, due to the low temperature threshold of the thermocouple. The temperature intervals chosen were room temperature (25 °C), 60 °C, 120 °C, 160 °C, and 200 °C. The temperature controller struggled to stabilise temperature at lower set temperature, therefore only one low temperature (60 °C) was chosen for investigation. For hydrogen terminations executed in the MWCVD reactor, the operating temperature is up to 900 °C. Therefore, it was thought that hydrogen termination would only become effective at much higher temperatures.

The four plasma times chosen to investigate at each temperature were 60 s, 180 s, 360 s, and 600 s. The oxygen-terminated surface is more stable than the hydrogen-terminated diamond. Because of this, the hydrogen-terminated surface is more labile to oxygen plasma than *vice*

*versa*. This is the reason why the plasma durations being investigated for hydrogen termination are much longer than previously investigated for oxygen termination. For efficiency of termination, it would be beneficial to find conditions that are balanced between plasma duration and substrate temperature.

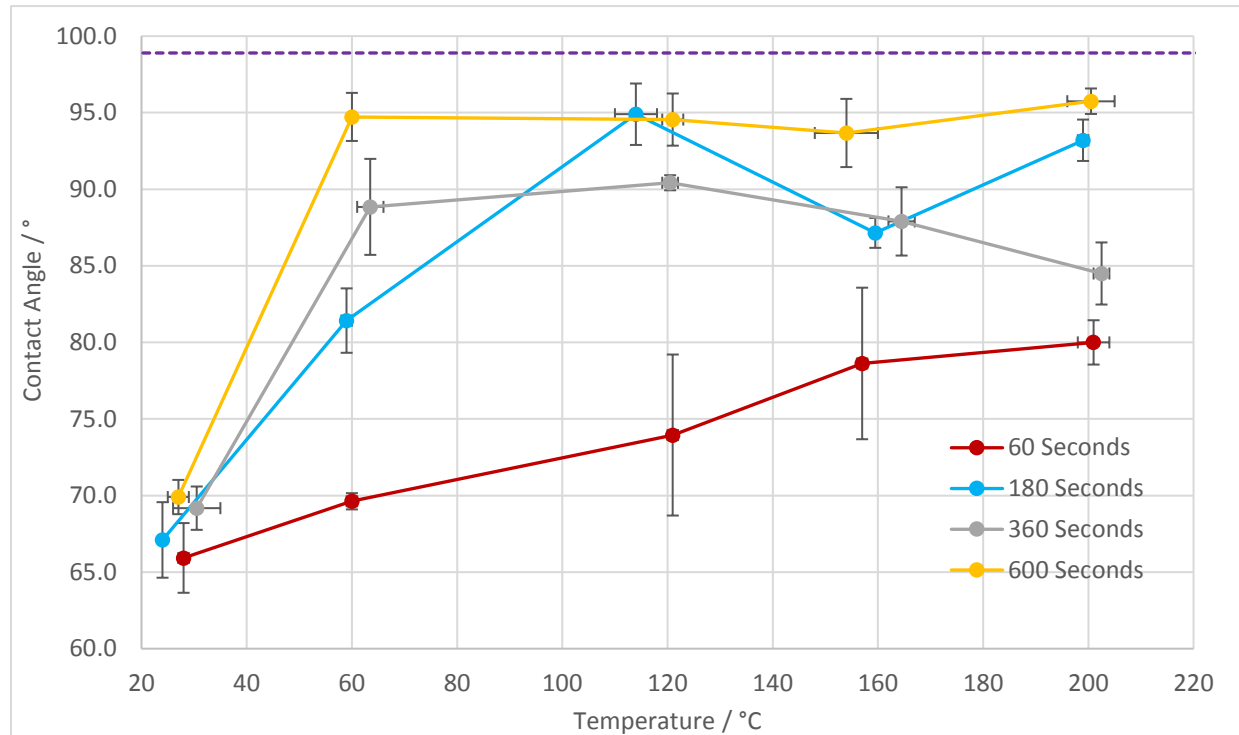


**Figure 26: The average surface contact angle as a function of temperature and plasma duration.**

The contact angle measurements are compared with the control hydrogen termination obtained using the MWCVD reactor ( $98.9^\circ \pm 4.5^\circ$ ). This is depicted by the dotted purple line in Fig. 26. As the hydrogen-terminated diamond surface is hydrophobic, it is assumed that a higher contact angle measurement indicates a higher hydrogen surface coverage.

From Fig. 26, it can be seen that at room temperature, increasing plasma duration has very little effect on the efficacy of hydrogen termination. However, for all four plasma durations, heating the substrate substantially increases the recorded contact angle. But, for samples terminated using the shortest plasma duration (60 s), heating to 200 °C still does not result in a contact angle comparable with the hydrogen-terminated control sample. The substrate heating had a much greater effect on hydrogen termination for longer plasma exposures (180 s, 360 s, 600 s), where a sharp increase occurs on increasing the substrate temperature to 60 °C. For each different plasma time series, the contact angle appears to plateau. Increasing the plasma

duration, causes the plateau to occur at a greater average surface contact angle. The diamond films exposed to 600 s of hydrogen plasma, produce the most comparable contact angles to the value obtained from the control sample. An exception to this is the resultant contact angle measurement for the hydrogen termination executed at 114 °C, using a 180 s plasma exposure ( $94.9^\circ \pm 2.0^\circ$ ).

Similar to the contact angle values obtained for the oxygen terminations, these measurements are accompanied by considerable uncertainty. The uncertainty for the contact angle measurements is a result of variation within the repeat measurements, and was obtained by calculating the standard deviation. The variation is possibly due to the inconsistent surface roughness of polycrystalline diamond, which can cause discrepancies in the measurements. Similarly, the substrate temperature also contained uncertainties. This was due to the plasma interfering with the thermocouple, resulting in variation of temperature, as the temperature controller was unable to operate correctly. An image of a water contact angle measurement taken using the DSA can be seen in Fig. 27. The water droplet is analysed using the program Advance, provided by Krüss. In this image, the calculated droplet shape is not in agreement with the actual droplet shape. This results in erroneous contact angle measurements. Results such as these were discarded, and repeats performed.

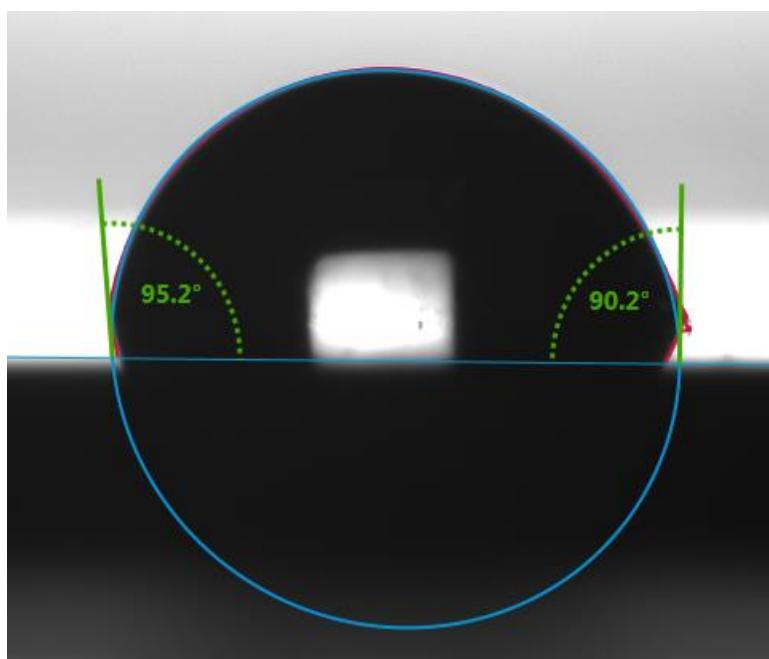


**Figure 27: Image of a 1.5 µL water droplet on the hydrogen-terminated surface. For this hydrogen termination, a plasma duration of 600 s and temperature of 154 °C was used. Image taken using the Krüss DSA, in conjunction with the Advance program.**

### 3.3.2.1 – Reproducibility

As mentioned previously, a water contact angle measurement matching the control sample ( $98.9^\circ \pm 4.5^\circ$ ) is a good indication of a full hydrogen surface coverage. None of the conditions used for hydrogen termination resulted in a contact angle equal to, or greater than the control sample. However, there were some conditions that resulted in contact angle measurements close to the control, or matching literature values for hydrogen termination of polycrystalline diamond film ( $93^\circ$ ). Repeat terminations were executed for the conditions that resulted in the most hydrophobic diamond surfaces. This was to ensure that the reactor was capable of reproducing the same quality of hydrogen termination. The results for the repeat terminations are displayed in Table 3.

**Table 3: Resultant contact angle measurements recorded for repeats of the conditions that originally gave contact angles closest to the control measurement ( $98.9^\circ$ ).**

Termination	Plasma Time / s	Temperature / °C	Contact Angle 1 / °	Contact Angle 2 / °	Contact Angle 3 / °	Average Contact Angle / °	Standard Deviation ( $\sigma$ )
Hydrogen	180	114	94.9	84.8	79.9	86.5	6.2
Hydrogen	600	121	94.6	85.6	87.0	89.1	4.0
Hydrogen	600	201	95.8	86.3	83.7	88.6	6.2

All of the repeat terminations resulted in considerably lower contact angle measurements compared to the initial contact angle measurements. This is reflected in the calculated standard deviation of the results. This indicates a poor ability to reproduce the same degree of hydrogen termination, even when using identical conditions.

### 3.3.2.2 – Discrepancies

The contact angle measurements were all accompanied by considerable uncertainties. Not only was there large variations in contact angle measurements within identical samples, but also considerable variation for repeat terminations completed using identical conditions. There are many possible explanations for such errors.

Both, the atomic composition of the surface and also the surface structure has an effect on water contact angle measurements. As mentioned previously, Wenzel analysed the effect of surface roughness on apparent surface contact angle ( $\theta$ ). The Wenzel equation (Eq. 4) shows that for hydrophobic surfaces (such as the hydrogen-terminated diamond surface), increased surface roughness, results in increased hydrophobicity.

All diamond films were synthesised using the HFCVD method, which led to a polycrystalline diamond film. The crystal facets in these films are roughly between 1 and 5  $\mu\text{m}$  in size, resulting in a surface area larger than the geometric area of the film ( $R_{\text{rough}} > 1$ ). This will give rise to an increased apparent contact angle compared to an atomically smooth hydrogen-terminated diamond film. The relative roughness ( $R_{\text{rough}}$ ) of each film could have been calculated using AFM. Utilising  $R_{\text{rough}}$ , the recorded contact angles ( $\theta_{\text{app}}$ ) could then be translated into the Young contact angle values ( $\theta_y$ ), quantifying the effect of surface roughness on contact angle. An assumption was made that all samples would have comparable roughness, and that surface roughness could be largely ignored, as the effect would be consistent across all readings. However, as no images of the samples were taken using AFM, it is not known if this correct.

Over the course of the project, these samples were routinely exposed to both oxygen and hydrogen plasma, both of which etch the diamond surface. Both oxygen and hydrogen plasma preferentially etch the (111) surface plane<sup>[69],[70]</sup>. All samples would have experienced similar amounts of plasma, and therefore similar etching. However, due to the preferential etching phenomenon, this would only be the case if the diamond surface topology is identical among samples. Also, larger, more protruding facets that formed during CVD growth, may have been disproportionately etched by plasma. All of these factors would have a large effect on surface roughness, thus contact angle measurements.

At room temperature, hydrogen-terminating atoms can be replaced by oxygen atoms. This is a slow process, but does occur in absence of heating. A possible source of error could therefore be the cooling of the samples. For hydrogen terminations, the samples are heated to as high as 200 °C. If the diamond films are not effectively cooled before exposure to air, there is a possibility of oxidation of the diamond surface. This would affect the surface contact angle

measurements. This may explain the lowering in contact angle measurements, at high temperature, for the 180 s plasma duration sample set.

## 4. – Conclusion

---

There were three main objectives to this project. The first of which was successfully growing CVD diamond films using the HF method. As shown by analysis using SEM and laser Raman spectroscopy, CVD diamond growth was successful, resulting in polycrystalline diamond films.

The second aim was to install a system within the DCPT reactor which enabled accurate substrate heating. Two heating cartridges were installed within the anode of the reactor chamber, in combination with a temperature controller. The system was effectively calibrated, allowing accurate control over the temperature at which the terminations are executed.

The third objective was to investigate the effect of heating the CVD diamond films on efficacy of hydrogen and oxygen termination using the DCPT reactor. The effect was quantified by using water contact angle measurements. Heating was found to have a negative effect on the efficacy of oxygen termination. The optimal conditions were found to be 7 seconds at room temperature. This is in agreement with previous research involving the DCPT reactor, which found the optimal conditions for oxygen termination to be a plasma time between 5 to 8 s at room temperature<sup>[66]</sup>.

For hydrogen termination, heating of the diamond substrate improved the resultant contact angle and hence, the efficacy of termination. However, no conditions could emulate the hydrophobicity displayed by the surface termination executed using the MWCVD reactor. It can therefore be assumed that the hydrogen coverage of samples terminated in the DCPT reactor, is lower. However, the variation between contact angles could be a result of error. Further tests, such as x-ray photoelectron spectroscopy (XPS) would need to be completed to quantify the exact hydrogen surface coverage.

Several sets of conditions resulted in promising contact angle measurements. However, repeat terminations using these conditions exhibited considerable deviation in contact angle measurements. There are many factors that could have led to the large variation in contact angle measurements. But, with the limited variety of tests executed, it is hard to pinpoint the exact issue. Perhaps one of the most likely sources of error is surface roughness. This could be

eliminated by repeating the surface terminations using both (100) and (111) single crystal diamond, as these are the predominant planes present in CVD diamond. Single crystal provides a much smoother surface, this can be further polished to remove surface roughness, and in turn remove error in the contact angle measurements.

## 5. – Further Work

---

### 5.1 – X-Ray Photoelectron Spectroscopy

The only analytical technique employed for surface analysis of the CVD diamond films was water contact angle measurements. This is only a qualitative method of looking at the surface termination, and therefore cannot provide an exact measurement value for the extent of hydrogen or oxygen termination. X-ray photoelectron spectroscopy (XPS) would allow an atomic breakdown of the surface layer of the CVD diamond films. Due to hydrogen atoms possessing no outer electrons, they cannot be viewed using XPS. However, it would be possible to analyse the oxygen-terminated diamond film. This could then be compared with the results from an analysed hydrogen-terminated diamond film to work out the extent of hydrogen coverage. Ideally the terminations would be executed on single crystal diamond, as XPS is more effective at analysing smooth surfaces<sup>[71]</sup>.

### 5.2 - Surface Position

During all prior terminations, the 1 × 1 cm diamond film samples were placed at the centre of the anode, and terminated individually. This was due to all the samples being subjected to varying plasma times and temperatures, and therefore it was unnecessary to execute multiple simultaneous terminations. However, if numerous samples all required terminations using the same conditions, investigation into the effect of sample position on the effective surface termination, would be essential.

Heating is completed using two cartridge heaters, embedded within the stainless steel anode. Due to stainless steel having a poor thermal conductivity ( $11-19 \text{ W m}^{-1} \text{ K}^{-1}$ ), dissipation of heat may be slow<sup>[72]</sup>. This would result in high temperatures in the area local to the heater cartridges and lower temperatures elsewhere. The plasma generated should be even across all areas of the anode. However, if the electrodes are not completely parallel, then the plasma may not be level. This would alter the effective contact of the plasma with the diamond sample and hence, the termination. To quantify the possible effects, further tests would need completing.

The future experiments would involve a set of oxygen-terminated diamond samples, placed at varying positions on the anode. Hydrogen termination would then be executed on the samples, at conditions that previously achieved the highest hydrogen coverage (600 s plasma time, 200 °C). The samples could then be analysed using water contact angle measurements, to determine if any position on the anode gets preferential hydrogen termination. This test could also be repeated, but instead with initially hydrogen-terminated diamond. These could then be placed on the anode at varying positions. The samples would then be oxygen terminated using the ideal conditions (7 s plasma time, 25 °C). Again, the effective termination could then be assessed using water contact angle measurements or XPS. This would give an insight into how even the plasma distribution is across the anode and whether the plasma-sample contact differs, depending on position.

### **5.3 - Cooling**

It was mentioned earlier that cooling could be a potential source of error. However, this was only a hypothesis. For the DCPT reactor to be a practical tool for hydrogen termination, it is important that the results are consistent. To do this, the variable of sample cooling needs to be considered. To quantify the effects of cooling, two sample sets would need to be completed. For one set, after termination is completed, the substrate would be cooled to room temperature before the reaction chamber is open and the samples exposed to air. To increase the rate of cooling, the pressure would be increased within the chamber by addition of hydrogen gas. The second samples would be terminated using identical conditions to the cooled set. However, instead of cooling the samples, they would be immediately exposed to air. The resultant contact angles for both samples could then be measured, and a comparison be made.

### **5.4 - Nitrogen Termination**

Succeeding the experimentation, the thermocouple in DCPT reactor was replaced for a model with much greater resistance to temperature. This allows exposing the diamond films to even higher temperatures during terminations. It is now conceivable that termination of the diamond film using nitrogen gas may be possible. Nitrogen gas is extremely stable due to the strong N-N triple bond. Because of this, termination using nitrogen gas is challenging. Even when a

nitrogen gas plasma is formed, it is more thermodynamically favourable for the nitrogen ions to reform nitrogen gas, rather than terminate the diamond surface. However, heating of the sample might possibly aid the process of nitrogen termination. Chandran *et al* reported successful nitrogen termination by annealing the diamond film to 1000 °C before exposing to N<sub>2</sub> radio frequency plasma<sup>[47]</sup>.

## 6. – References

---

- [1] – K.E. Spear and J.P. Dismukes, *Synthetic Diamond: Emerging CVD Science and Technology*, Wiley, Chichester, 1994
- [2] – A. Gicquel, K. Hassoumi, F. Silva and J. Achard, *CVD Diamond Film: From Growth to Applications*, *Curr. Appl. Phys.*, **1** (2001), 479-496
- [3] – Z. Yin, Z. Akkerman, B. X. Yang and F. W. Smith, *Optical Properties and Microstructure of CVD Diamond Films*, *Diamond Relat. Mater.*, **6** (1997), 153-158
- [4] - F.G. Celii and J. E. Butler, *Diamond Chemical Vapor Deposition*, *Annu. Rev. Phys. Chem.*, **42** (1991), 643-684
- [5] - K. Nassau and J. Nassau, *The History and Present Status of Synthetic Diamond*, *J. Cryst. Growth*, **46** (1979), 157-172
- [6] – J. C. Angus and C. C. Hayman, *Low-Pressure, Metastable growth of Diamond and “Diamondlike” Phases*, *Science*, **241**, 1988, 913-921
- [7] - M.N.R. Ashfold, P.W. May, C.A. Rego and N.M. Everitt, *Thin Film Diamond by Chemical Vapour Deposition Methods*, *Chem. Soc. Rev.*, **23** (1994), 21-29
- [8] - P.W. May, *Diamond Thin Films: A 21st Century Material*, *Phil. Trans. R. Soc. Lond. A*, **358** (2000), 473-495.
- [9] - S. J. Sque and R. Jones, *Structure, Electronics, and Interaction of Hydrogen and Oxygen on Diamond Surfaces*, *Phys. Rev. B*, **73** (2006), 085313
- [10] – F. Shimura, *Semiconductor Silicon Crystal Technology*, Academic Press Limited, London, 1<sup>st</sup> edn, 1989, ch. 3, 22-33
- [11] - X. Luo, Z. Liu, B. Xu, D. Yu, Y. Tian, H. Wang and J. He, *Compressive Strength of Diamond from First-Principles Calculation*, *J. Phys. Chem. C*, **114** (2010), 17851-17853
- [12] - M. De La Pierre, M. Bruno, C. Manfredotti, F. Nestola, M. Prencipe and C. Manfredotti, *The (100), (111) and (110) Surfaces of Diamond: an Ab Initio B3LYP Study*, *Mol. Phys.*, **112** (2014), 1030-1039
- [13] – J. Ristein, *Diamond Surfaces: Familiar and Amazing*, *Appl. Phys. A*, **82** (2006), 377-384
- [14] - G. Kern, J. Hafner and G. Kresse, *Atomic and Electronic Structure of Diamond (111) Surfaces I. Reconstruction and Hydrogen De-reconstruction of the One Dangling-Bond Surface*, *Surf. Sci.*, **366** (1996), 445-463
- [15] – P. K. Baumann and R. J. Nemanich, *Surface Cleaning, Electronic States and Electron Affinity of Diamond (100), (111) and (110) Surfaces*, *Surf. Sci.*, **409** (1998), 320-335
- [16] – R. E. Stallcup, A. F. Aviles and J. M. Perez, *Atomic Resolution Ultrahigh Vacuum Scanning Tunneling Microscopy of Epitaxial Diamond (100) Films*, *Appl. Phys. Lett.*, **66** (1995), 2331
- [17] - A. Scholze, W. G. Schmidt and F. Bechstedt, *Structure of the Diamond (111) Surface: Single-Dangling-Bond Versus Triple-Dangling-Bond Face*, *Phys. Rev. B*, **53** (1996), 13725-13733
- [18] – N. Tokuda, H. Umezawa, K. Yamabe, H. Okushi and S. Yamasaki, *Growth of Atomically Step-Free Surface on Diamond {111} Mesas*, *Diamond Relat. Mater.*, **19**, 2010, 288-290
- [19] - M.C. Salvadori, W.W.R. Arujo, F.S. Teixeira, M. Cattani, A. Pasquarelli, E.M. Oks and I.G. Brown, *Termination of Diamond Surfaces with Hydrogen, Oxygen and Fluorine Using a Small, Simple Plasma Gun*, *Diamond Relat. Mater.*, **19** (2010), 324-328
- [20] – L. Feng-Bin, W. Jia-Dao, C. Da-Rong and Y. Da-Yum, *Electronic Properties of Hydrogen- and Oxygen-Terminated Diamond Surfaces Exposed to the Air*, *Chin. Phys. Soc.*, **18** (2009), 2041-2047
- [21] - V. Seshan, D. Ullien1, A. Castellanos-Gomez, S. Sachdeva, D. H. K. Murthy, T. J. Savenije, H. A. Ahmad, T. S. Nunnay, S. D. Janssens, K. Haenen, M. Nešládek, H. S. J. van der Zant, E. J. R. Sudhölter, and L. C. P. M. de Smet, *Hydrogen Termination of CVD Diamond Films by High-Temperature annealing at Atmospheric pressure*, *J. Chem. Phys.*, **138** (2013), 234707
- [22] – J. S. Foord, L. C. Hian and R. B. Jackman, *An Investigation of the Surface reactivity of Diamond Photocathodes with Molecular and Atomic Oxygen Species*, *Diamond Relat. Mater.*, **10** (2001), 710-714

- [23] - T. Ando, K. Yamamoto, M. Ishii, M. Kamo and Y. Sato, *Vapour-Phase Oxidation of Diamond Surfaces in O<sub>2</sub> Studied by Diffuse Reflectance Fourier-Transform Infrared and Temperature-Programmed Desorption Spectroscopy*, *J. Chem. Soc., Faraday Trans.*, **89** (1993), 3635-3640
- [24] - I. L. Krainisky, V. M. Asnin, G. T. Mearini and J. A. Dayton Jr., *Negative-Electron-Affinity Effect on the Surface of Chemical-Vapor-Deposited Diamond Polycrystalline Films*, *Phys. Rev. B*, **53** (1996), 7650-7653
- [25] - K. M. O'Donnell, T. L. Martin, M. T. Edmonds, A. Tadich, L. Thomsen, J. Ristein, C. I. Pakes, N. A. Fox and L. Ley, *Photoelectron Emission from Lithiated Diamond*, *Phys. Status Solidi A*, **211** (2014), 2209-2222
- [26] - I. L. Krainisky and V. M. Asnin, *Negative Electron Affinity Mechanism for Diamond Surfaces*, *Appl. Phys. Lett.*, **72** (1998), 2574-2576
- [27] - A. L. Allred, *Electronegativity Values from Thermochemical Data*, *J. Inorg. Nucl. Chem.*, **17** (1961), 215-221
- [28] - A. K. Tiwari, J. P. Goss, P. R. Briddon, N. G. Wright, A. B. Horsfall, R. Jones, H. Pinto and M. J. Rayson, *Calculated Electron Affinity and Stability of Halogen-Terminated Diamond*, *Phys. Rev. B*, **84** (2011), 245305
- [29] - C. Bandis and B.B. Pate, *Photoelectric Emission from Negative-Electron-Affinity Diamond (111) Surfaces: Exciton Breakup Versus Conduction-Band Emission*, *Phys. Rev. B*, **52** (1995), 12056-12071
- [30] - L.K. Bigelow and M.P. D'Evelyn, *Role of Surface and Interface Science in Chemical Vapor Deposition Diamond Technology*, *Surf. Sci.*, **500** (2002), 986-1004
- [31] - K. P. Loh, X. N. Xie, S. W. Yang and J. C. Zheng, *Oxygen Adsorption on (111)-Oriented Diamond: A Study with Ultraviolet Photoelectron Spectroscopy, Temperature-Programmed Desorption, and Periodic Density Functional Theory*, *J. Phys. Chem. B*, **106** (2002), 5230-5240
- [32] - D. Petrini and K. Larsson, *A Theoretical Study of the Energetic Stability and Geometry of Hydrogen- and Oxygen-Terminated Diamond (100) Surfaces*, *J. Phys. Chem. C*, **111** (2007), 795-801
- [33] - P. E. Pehrsson and T. W. Mercer, *Oxidation of the Hydrogenated Diamond (100) Surface*, *Surf. Sci.*, **460** (2000), 49-66
- [34] - G. Speranza, S. Torrenzo, A. Miotello, L. Minati, I. Bernagozzi, M. Ferrari, M. Dipalo, E. Kohn, *XPS and UPS in situ Study of Oxygen thermal desorption from Nanocrystalline Diamond Surface Oxidized by Different Process*, *Diamond Relat. Mater.*, **20** (2011), 560-563
- [35] - F. Klauser, S. Ghodbane, R. Boukherroub, S. Szunerits, D. Steinmuller-Nethl, E. Bertel and N. Memmel, *Comparison of Different Oxidation Techniques on Single-Crystal and Nanocrystalline Diamond Surfaces*, *Diamond Relat. Mater.*, **19** (2010), 474-478
- [36] - L. Mayrhofer, G. Moras, N. Mulakaluri, S. Rajagopalan, P. A. Stevens and M. Moseler, *Fluorine-Terminated Diamond Surfaces as Dense Dipole Lattices: The Electrostatic Origin of Polar Hydrophobicity*, *J. Am. Chem. Soc.*, **138** (2016), 4018-4028
- [37] - K. J. Rietwyk, M. Wanke, H. M. Vulling, M. T. Edmonds, P. L. Sharp, Y. Smets, Q.H. Wu, A. Tadich, S. Rubanov, P. J. Moriarty, L. Ley and C. I. Pakes, *Fluorination of the Diamond Surface by Photoinduced Dissociation of C<sub>60</sub>F<sub>48</sub>*, *Phys. Rev. B*, **84** (2011), 035404
- [38] - F. G. Sen, Y. Qi and A. T. Alpas, *Surface Stability and Electronic Structure of Hydrogen- and Fluorine-Terminated Diamond Surfaces: A First Principles investigation*, *J. Mater. Res.*, **24** (2009), 2461-2470
- [39] - K. Larsson and S. Lunell, *Stability of Halogen-Terminated Diamond (111) surfaces*, *J. Phys. Chem. A*, **101** (1997), 76-82
- [40] - A. Freedman and C. D. Stinespring, *Fluorination of Diamond (100) by Atomic and Molecular Beams*, *Appl. Phys. Lett.*, **57** (1990), 1194-1196
- [41] - F. Morar, F.J. Himpsel, G. Hollinger, J.L. Jordan, G. Hughes and F.R. McFeely, *C 1s Excitation Studies of Diamond (111). I. Surface Core Levels*, *Phys. Rev. B*, **33** (1986), 1340-1345
- [42] - V. S. Smentkowski and J. T. Yates Jr., *Fluorination of Diamond Surfaces by Irradiation of Perfluorinated Alkyl Iodides*, *Science*, **271** (1996), 193-195
- [43] - J. C. Biffinger, H. W. Kim and S. G. DiMugno, *The Polar Hydrophobicity of Fluorinated Compounds*, *ChemBioChem*, **5** (2004), 622-627

- [44] – D. Zhu, J. A. Bandy, S. Li and R. J. Hamers, *Amino-Terminated Diamond Surfaces: Photoelectron Emission and Photocatalytic Properties*, *Surf. Sci.*, **650** (2016), 295-301
- [45] – T. Kageura, K. Kato, H. Yamano, E. Suaebah, M. Kajiya, S. Kawai, M. Inaba, T. Tanii and M. Haruyama, *Effect of a Radical Exposure Nitridation Surface on the Charge Stability Shallow Nitrogen-Vacancy Centers in Diamond*, *Appl. Phys. Express*, **10** (2017), 055503
- [46] – K.I. Sotowa, T. Amamoto, A. Sobana, K. Kusakabe and T. Imato, *Effect of treatment Temperature on the Amination of Chlorinated Diamond*, *Diamond Relat. Mater.*, **13** (2004), 145-150
- [47] – M. Chandran, M. Shasha, S. Michaelson and A. Hoffman, *Nitrogen Termination of Single Crystal (100) Diamond Surface by Radio Frequency N<sub>2</sub> Plasma Process: An in-situ X-Ray Photoemission Spectroscopy and Secondary Electron Emission Studies*, *Appl. Phys. Lett.*, **107** (2015), 111602
- [48] – J.P. Chou, A. Retzker and A. Gali, *Nitrogen-Terminated Diamond (111) Surface for Room-Temperature Sensing and Simulation*, *Nano Lett.*, **17** (2017), 2294-2298
- [49] – V. Vermeeren, S. Wenmackers, P. Wagner and L. Michiels, *DNA Sensors with Diamond as a Promising Alternative Transducer Material*, *Sensors*, **9** (2009), 5600-5636
- [50] – G.J. Zhang, K.S. Song, Y. Nakamura, T. Ueno, T. Funatsu, I. Ohdomari and H. Kawarada, *DNA Micropatterning on Polycrystalline Diamond via One-Step Direct Amination*, *Langmuir*, **22** (2006), 3728-3734
- [51] – C. Stavis, T. L. Clare, J. E. Butler, A. D. Radadia, R. Carr, H. Zeng, W. P. King, J. A. Carlisle, A. Aksimentiev, R. Bashir and R. J. Hamers, *Surface Functionalization of Thin-Film Diamond for Highly Stable and Selective Biological Interfaces*, *PNAS*, **108** (2011), 983-988
- [52] – C.E. Nebel, D. Shin, D. Takeuchi, T. Yamamoto, H. Watanabe and T. Nakamura, *Photochemical Attachment of Amine Linker Molecules on Hydrogen Terminated Diamond*, *Diamond Relat. Mater.*, **15** (2006), 1107-1112
- [53] – Q. Wang, A. Kromka, J. Houdkova, O. Babchenko, B. Rezek, M. Li, R. Boukherroub and S. Szunerits, *Nanomolar Hydrogen Peroxide Detection Using Horseradish Peroxidase Covalently Linked to Undoped Nanocrystalline Diamond Surfaces*, *J. Am. Chem. Soc.*, **28** (2012), 587-592
- [54] – Y. L. Zhong, K. P. Loh, A. Midya and Z.K. Chen, *Suzuki Coupling of Aryl Organics on Diamond*, *Chem. Mater.*, **20** (2008), 3137-3144
- [55] – W. S. Yeap, D. Bevk, X. Liu, H. Krysova, A. Pasquarelli, D. Vanderzande, L. Lutsen, L. Kavan, M. Fahlman, W. Maes and K. Haenen, *Diamond Functionalisation with Light Harvesting Molecular Wires: Improved Surface Coverage by Optimised Suzuki Cross-Coupling Conditions*, *RSC Adv.*, **4** (2014), 42044-42053
- [56] – J. S. Foord, C. H. Lau and M. Hiramatsu, *Transmissive Diamond Photocathodes*, *Carbon*, **43** (2005), 2106-2111
- [57] – K. Okano, K. Hoshina, M. Iida, S. Koizumi and T. Inuzuka, *Fabrication of a Diamond Field Emitter Array*, *Appl. Phys. Lett.*, **64** (1994), 2742-2744
- [58] – M. C. Kan, J. L. Huang, J. C. Sung, K. H. Chen and B. S. Yau, *Thermionic Emission of Amorphous Diamond and Field Emission of Carbon Nanotubes*, *Carbon*, **41** (2003), 2839-2845
- [59] – K. M. O'Donnell, T. L. Martin, N. A. Fox and D. Cherns, *Ab Initio Investigation of Lithium on the Diamond C(100) surface*, *Phys. Rev. B*, **82** (2010), 115303
- [60] – K. M. O'Donnell, T. L. Martin and N. L. Allan, *Light Metals on Oxygen-Terminated Diamond (100): Structure and Electronic Properties*, *Chem. Mater.*, **27** (2015), 1306-1315
- [61] – K. M. O'Donnell, M. T. Edmonds, A. Tadich, L. Thomsen, A. Stacey, A. Schenk, C. I. Pakes and L. Ley, *Extremely High Negative Electron Affinity of Diamond via Magnesium Adsorption*, *Phys. Rev. B*, **92** (2015), 035303
- [62] – H.J. Butt, K. Graf and M. Kappl, *Physics and Chemistry of Interfaces*, Wiley-VCH, Weinheim, 3<sup>rd</sup> edn, 2013, ch. 6, 143-180
- [63] – D.Y. Kwok and A.W. Neumann, *Contact Angle Measurement and Contact Angle Interpretation*, *Adv. Colloid Interface Sci.*, **81** (1999), 167-249
- [64] – L. Ostrovskaya, V. Perevertailo, V. Ralchenko, A. Dementjev and O. Liginova, *Wettability and Surface Energy of Oxidized and Hydrogen Plasma-Treated Diamond Films*, *Diamond Relat. Mater.*, **11** (2002), 845-850

- [65] - M. Mertens, M. Mohr, K. Brühne, H.J. Fecht, M. Łojkowski, W. Świążzkowski and W. Łojkowski, *Patterned Hydrophobic and Hydrophilic Surfaces of Ultra-Smooth Nanocrystalline Diamond Layers*, *Appl. Surf. Sci.*, **390** (2016), 526-530
- [66] – J. Bird, MSci Thesis, Studying the Oxidation of Diamond Using an O<sub>2</sub> Plasma Reactor, 2017
- [67] – T. Al-Jeda, MSci Thesis, Contruction and Operation of a Plasma System to Fluorinate and Aminate the Surfaces of Diamond Thin Films, 2018
- [68] – S. Praver and R. J. Nemanich, *Raman Spectroscopy of Diamond and Doped Diamond*, *Phil. Trans. R. Soc. Lond. A*, **362** (2004), 2537-2565
- [69] – Z. Shpilman, I. Gouzman, E. Grossman, R. Akhvlediani and A. Hoffman, *Hydrogen Plasma and Atomic Oxygen Treatments of Diamond: Chemical Versus Morphological Effects*, *Appl. Phys. Lett.*, **92** (2008), 234103
- [70] – M. Wolfer, J. Biener, B.S. El-Dasger, M. Biener, A. V. Hamza, A. Kriele and C. Wild, *Crystallographic Anisotropy of Growth and Etch Rates of CVD Diamond*, *Diamond Relat. Mater.*, **18** (2009), 713-717
- [71] – L.S. De Bernardez, J. Ferrón, E.C. Goldberg and R.H. Buitrago, *The Effect of Surface Roughness on XPS and AES*, *Surf. Sci.*, **139** (1984), 541-548
- [72] – M.F. Ashby, *Materials Selection in Mechanical Design*, Butterworth-Heinemann, Oxford, 2<sup>nd</sup> edn, 1999, ch 4, 45-79